Staircase fractures in microbialites and the role of lamination-related mechanical anisotropy: The example of the Acquasanta Terme travertine deposits (central Italy)

Matteo Maggi[1,†], Paola Cianfarra[1], Francesco Salvini[1], and Claudio Coelho de Lima[2]
[1]*Dipartimento di Scienze–Sezione Geologia, Università degli Studi Roma Tre, Largo San Leonardo Murialdo 1, 00146, Roma, Italy*
[2]*Petrobras S/A, Avenida República do Chile 65, 20031-912, Centro Rio de Janeiro, Brazil*

ABSTRACT

This study describes a peculiar, yet common type of fracture showing a staircase trajectory, which forms in rocks with moderately weak planar anisotropies. The staircase fracture trajectory is given by alternating fracture segments oriented parallel to (LaP) or at an angle (ramp) with respect to the lamination/layering. The analyses has been accomplished on travertines, which are continental microbial/hydrothermal deposits having a typical poorly stratified yet strongly laminated texture. In these rocks, porosity and permeability have a high across-lamination variability and are mostly controlled by an interconnected and locally corroded array of permeable layers, fractures, and faults. Structural analysis integrated with analytical modeling provided a conceptual model of staircase fracture localization as a function of the travertine lamination dip. Lamination-parallel fracture segments localize within the porous laminae, mostly at the interface with tight laminae. Ramp-type fracture segments cut the lamination, connecting lamination parallel segments. Two types of staircase fracture can be modeled. The first group develops in subhorizontal to gently dipping deposits (lamination dip < 30°) corresponding to low-energy depositional environments. The second group relates to staircase fractures developed in moderately to steeply dipping laminations (lamination dip >30°) and corresponds to high-energy environments. Major discoveries of hydrocarbon have been recently made in continental (lacustrine) microbial carbonates in the Brazilian South Atlantic margin, some of which exhibit a texture similar to those usually observed in travertines. Understanding of the lacustrine carbonates is still at an early stage. Given that in modern rift settings, vent-related thermal (travertine) and nonthermal (tufa) carbonates are a major component, the proposed conceptual model of staircase fracture localization contributes to the preparation of a model for the potential occurrence of high-permeability pathways in hydrocarbon and geothermal microbial reservoirs.

INTRODUCTION

Fractures systems strongly affect rock permeability by enhancing pore interconnectivity (Gross and Eyal, 2007; Larsen et al., 2010; Larsen and Gudmundsson, 2010). Understanding and predicting fracture pattern geometry, distribution, and interconnection in carbonates reservoirs represent relevant goals in the water supply (e.g., Cooke et al., 2006), oil and gas (Hennings, 2009), and geothermal industries. There is increasing interest in the study of the origin and development of marine to continental (lacustrine) microbial carbonates after the recent discovery of hydrocarbons along the South Brazilian Atlantic margin (Carminatti et al., 2008; Wright, 2012; Mancini et al., 2013). One of the major point regards the texture and fabric of microbialites, which influence porosity and permeability of the reservoir (Mancini et al., 2013). Porosity and permeability in microbialites vary with facies and are strongly controlled by the degree and kind of diagenesis, and fracturing (Ahr, 2008, 2009). The lateral continuity of the porous layer is variable, and porous layers may be enveloped by tight micritic carbonates.

Independently from the depositional process or the environment, microbialites are massive deposits characterized by the alternation of tight nonlaminated and porous finely laminated layers (Flügel, 2004; Riding, 2011). This alternation is produced by the feedback between biological activity (both algal and microbial) and physico-chemical processes, externally tuned by climate variability and tectonics (Chafetz and Folk, 1984; Fouke et al., 2003; Anzalone, 2008; Faccenna et al., 2008; Amato et al., 2012; Brogi et al., 2012; Ascione et al., 2013; Mancini et al., 2013).

Lamination is defined as a very thin planar structure (<1 cm) produced by a variation in the deposition conditions (mineralogical composition, grain size, texture, etc.) that do not involve an interruption in the sedimentation (Flügel, 2004). Nevertheless the distinction from stratification, characterized instead by recognizable boundary planes, is not well defined.

Hereby, lamination and stratification are distinguished by their strength contrast. Lamination is characterized by a subordered strength contrast between laminae with respect to that between strata and interstrata. The typical framework of these laminated, thick benches is show in Figure 1.

The strength contrast produced by sedimentary structures deeply influences the development and pattern of brittle deformation in carbonate rocks (Becker and Gross, 1996; Di Naccio et al., 2005; Cooke et al., 2006; Tavani et al., 2008; Laubach et al., 2009; Larsen and Gudmundsson, 2010; Ortega et al., 2010; Barbier et al., 2012). In this study we show how in microbialites the interaction between the acting stresses and the strength contrast at the boundaries between porous and tight layers (lamination) results in the development of fractures following a characteristic staircase trajectory (Fig. 2). These fracture patterns are commonly observed in sedimentary environments and are strongly influenced by the internal sedimentary structures (de Wet et al., 1999, and reference therein; Xianghua and Ming, 2002). The term staircase is here adopted to describe these fracture trajectories, following Eisenstadt and De Paor (1987), which first used this term, although in another context, to describe thrust-fault propagation in alternating weak and strong rock units.

Travertines and tufas are commonly included in the microbialites category after the identification of the primary role of bacterial activity in their

[†]matteo.maggi@uniroma3.it.

doi: 10.1130/B31163.1; 16 figures; 2 tables.

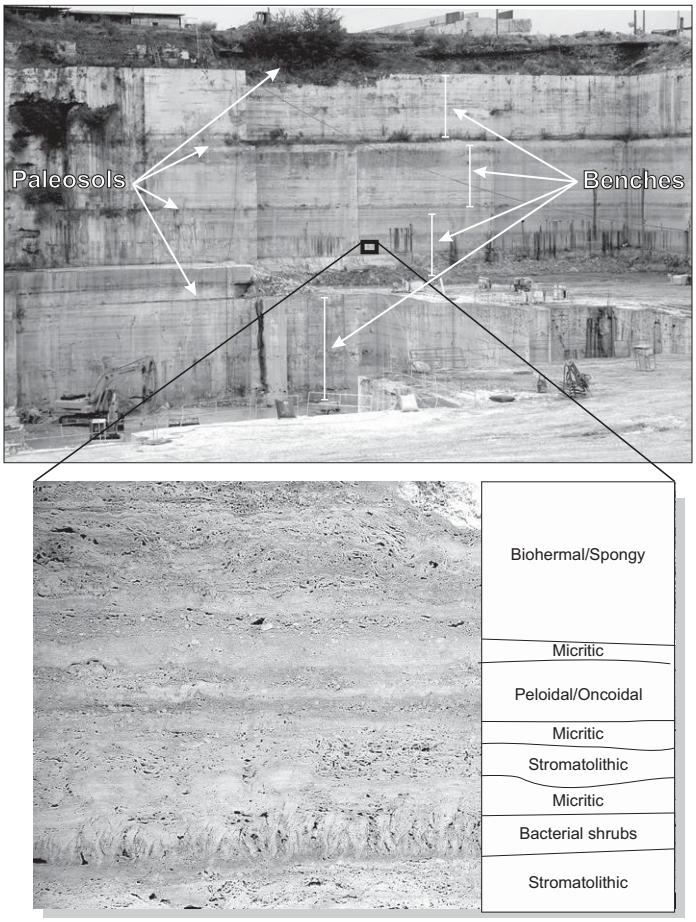

Figure 1. Laminated benches in travertines (Tivoli, Rome). In this example, benches are delimitated by paleosols. The enlarged picture shows the main travertine microfacies responsible for the internal bench lamination. Note the alternation between porous/permeable levels (stromatolite, shrubs, biohermal/spongy) and low-permeability/impermeable levels (micrite, peloidal/oncoidal).

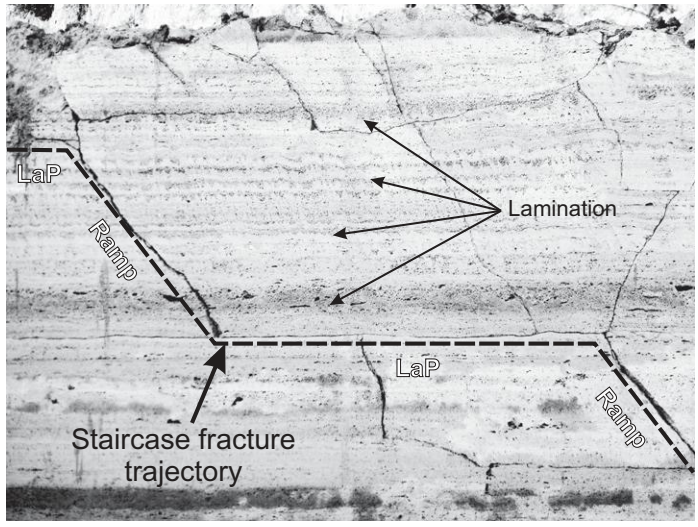

Figure 2. Examples of staircase fractures in microbialites (Acquasanta Terme, central Italy), showing the ramp and lamination/layer-parallel (LaP) segments.

formation (Chafetz and Folk, 1984; Koban and Schweigert, 1993). With their characteristic poorly stratified yet strongly laminated texture, travertines represent a natural laboratory in which to understand the relationships among acting stresses, sedimentary structures, and resulting fracture architecture. Detailed classification of microbialites and travertines microfacies is far beyond the purpose of this paper, which is focused on the role of mechanical anisotropy produced by the alternation of porous and tight laminae on fracture development.

This study describes and proposes a conceptual model of the observed staircase fractures (staircase fracture, Fig. 2) in the Quaternary travertine deposits outcropping in the region of the Acquasanta Terme town (central Italy; Boni and Colacicchi, 1966; Farabollini et al., 2005), a moderately deformed deposit that shows a high variability of depositional environments allowing us to provide a general scheme for fracture formation in microbialites.

As thermal water springs are still present (Galdenzi et al., 2010), the Acquasanta Terme location has been tested for its geothermal potential (Madonna et al., 2005; Menichetti, 2008; Fusari et al., 2013). Travertines are a class of microbial buildups associated with vents/faults (Chafetz and Folk, 1984; Wright, 2012) showing striking textural similarity between the shrub-like structures found in travertines and in microbial carbonates reservoirs discerned by Wright (2012). We propose that the Acquasanta travertines can be used as an analogue for the characterization of the porosity and permeability in both hydrocarbon and geothermal fluid reservoirs.

GENERAL CONSIDERATIONS ON TRAVERTINES

Travertines sensu lato represent the main continental carbonates deposits (Pentecost, 1995; Fouke et al., 2000; D'Argenio, 2001; D'Argenio and Ferreri, 2004; Golubić et al., 2008). Travertines are deposited along vent-controlled springs and result from both inorganic and organic processes: In the vicinity of the spring, hot and acid waters favor the rapid inorganic precipitation of carbonates upon degassing, whereas bacterial-induced precipitation prevails down current, as water temperature reaches the optimum temperature (21–23 °C). The amelioration of the environmental conditions allows the further establishment of blue-green algae, and then the higher taxa of plants (Chafetz and Folk, 1984). Where vents are associated with shallow lakes, a major component of travertine outcrops is decimeter-thick laterally continuous alternating layers with carbonate muds and shrub-like structures (Fig. 1). Wright (2012) stated that the shrub-like structures found in travertines are remarkably similar to those found in microbial carbonates of the Campos and Santos basin, previously published by Terra et al. (2009) and Dias (2005).

Several partly contrasting classifications are present in the literature and based on textural, environmental gradient, and/or geochemical parent water characteristics (Koban and Schweigert, 1993; Pentecost and Viles, 1994; Ford and Pedley, 1996; Gandin et al., 2008). Some authors limit the term travertine to indicate the massive and less porous deposits, as distinguished from calcareous tufa, which are the poorly cemented and more pourous ones (e.g., Gandin et al., 2008). This subdivision is deeply influenced by diagenesis (both early and late) and compaction processes (Anzalone, 2008; Golubić et al., 2008; Amato et al., 2012). A distinction is done also from the parent water origin, temperature, and the relative biodiversity (Anzalone et al., 2007). Travertine deposition in temperate climates relates generally to thermal water springs and associated microbial activity. Calcareous tufas relate to surface water temperature and the presence of macrophyta (i.e., ambient water; sensu Anzalone et al., 2007)

The sedimentary organization of different travertine and calcareous tufa deposits shows similar gross features (Anzalone, 2008), and a continuous transition from travertines to calcareous tufa has been commonly observed (Capezzuoli et al., 2008; Brogi et al., 2012; Wright, 2012). These observations suggest that travertines and calcareous tufa might be considered as end members of a complex depositional system involving multiple factors such as tectonics, climate, geochemistry and biological activity. The term travertine is hereby used to cover a range of continental carbonate sedimentary processes along a temperature gradient (Golubić et al., 2008).

In addition, travertine deposition relates to active tectonics and faulting, which provide the main conduits for Ca-rich hydrothermal fluid upwelling (Fig. 3; Platt and Wright, 1991; Hancock et al., 1999; Minissale et al., 2002; Brogi et al., 2012; De Filippis et al., 2012, 2013a). This is confirmed by the occurrence of present-day travertine deposition also in tectonically controlled Arctic environments (Cianfarra and Salvini, 2014, and reference therein). Often, travertines are deposited along active faults, the activity of which is responsible for their syn- to postdeposition diagenesis and deformation (De Filippis et al., 2012, 2013b). The interaction between tectonics and travertine deposition includes crack sealing and reopening (De Filippis et al., 2012, and reference therein). The role of fault activity is also necessary to maintain an active depocenter and a topographic gradient to allow surficial fluid flow.

Travertine lithofacies and their association allow us to recognize the depositional environments (Anzalone et al., 2007). Depositional environments are characterized by different energy and dynamic regimes of the water flow from plateau to lake-to-marsh, to slope, to waterfall deposits (Platt and Wright, 1991; D'Argenio et al., 2008). The upward growth of the encrustation gradually tends to lower the original slope angle (Anzalone et al., 2007; D'Argenio et al., 2008), resulting in flattening zones with increasingly steeper margins in which braided channeling laterally evolves into waterfalls, while flattened top areas support ponds and shallow lakes. In an ideal section, different flow regimes with increasing energy lead to the deposition from incoherent/lousy deposits (low-energy flow regime, i.e., shallow lake to pond environments; sl of Fig. 3), to poorly sustained slope deposits (draped and cross-lamination facies, intermediate-energy flow regime; gs and hm of Fig. 3), to the self-sustained hydrothermal mound, waterfall, and pool and dam environment (high-energy flow regime; wp of Fig. 3). Depending on depositional processes and environment, porous and permeable structures can be formed, including bacterial shrubs and shrub-like (arborescent), biohermal, spongy, peloidal/oncoidal grainstones, and stromatolitic (microbialites sensu stricto) facies (Mancini et al., 2013, and reference therein)

The fast grow rate of travertine deposits (up to 5 mm/d; Fouke et al., 2003) results in the development of rather homogeneous benches (Fig. 1), up to several meters thick, interrupted by erosional surfaces and paleosols often related to climatic events (Anzalone et al., 2007; Faccenna et al., 2008). The lateral extent of single benches is highly variable and often limited to few tens of meters. On the other hand, the incrustation style of deposition commonly produces a very fine internal lamination defined by the alternation of porous versus tight laminae (Pentecost, 2005).

From the mechanical stratigraphy point of view, benches can be assimilated to strata since the interleaved erosional surfaces offer a marked strength contrast with respect to lamination. The thickness of travertine benches makes these rocks particularly suited to study the effect of lamination on fracture patterns and propagation.

GEOLOGICAL SETTINGS

The Acquasanta travertine deposits (Boni and Colacicchi, 1966; Farabollini et al., 2005) are located in the Marche region (central Italy, Fig. 4) on the eastern side of the Northern Apennine Chain.

The Apennine Chain is an E-verging thrust-and-fold belt resulting from the convergence of the Eurasia and Adria-Africa plates during the Cenozoic and the successive Tyrrhenian Sea opening in Miocene time (e.g., Ogniben et al., 1975; Royden et al., 1987; Carmignani et al., 1995). It mainly involves Mesozoic–Cenozoic, shallow- to deep-water carbonates developed in a passive margin environment, where synsedimentary extensional faulting controlled the distribution of structural highs and depocenters since the Upper Triassic (Ciarapica and Passeri, 2002; Calamita et al., 2011, and references therein). Carbonate successions are topped by Miocene–Pliocene synorogenic siliciclastic successions that constitute the foredeep deposits (e.g., Principi and Treves, 1984; Boccaletti et al., 1990; Bigi et al., 1999). The timing of the early stages of the Apennine belt development is late Eocene times (e.g., Maggi et al., 2012, and references

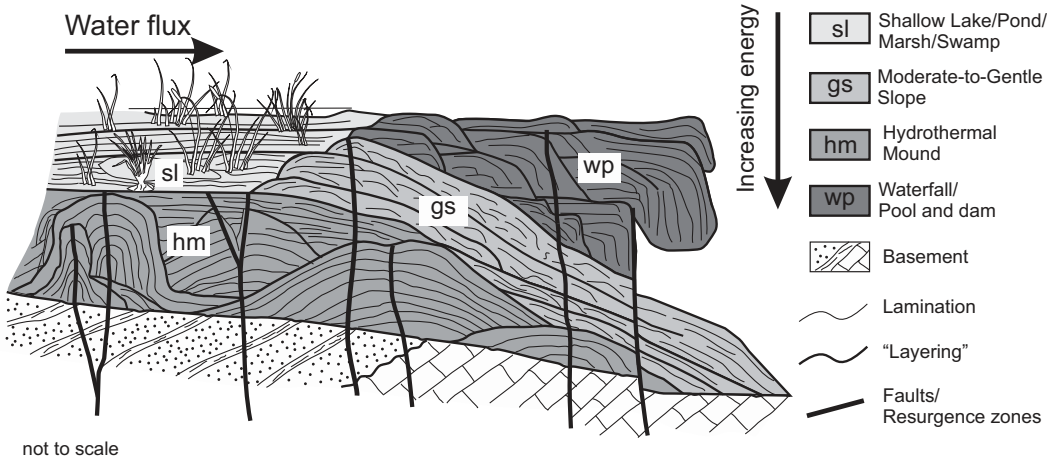

Figure 3. Synthetic cartoon representing the observed depositional environments and their geometric relationships in the thermal-to-freshwater travertine deposits of Acquasanta Terme from a comparison of several authors (Platt and Wright, 1991; Ford and Pedley, 1996; Fouke et al., 2000; Anzalone, 2008; Capezzuoli et al., 2008; D'Argenio et al., 2008). As parent water temperature decreases, the system evolves from travertine sensu stricto in hydrothermal mounds (hm) to calcareous tufa in marsh, swamp, and shallow lake environments (sl). Moderate-to-gentle slope (gs) and pool and dam/waterfall (wp) represent intermediate environments. The basement original slope is progressively obliterated to flat zones on top and steep zones on the front by aggrading/prograding deposition. This produces the observed dual behavior in travertine depositional systems, where high- energy environments coexist with low-energy environments. Faulting plays a primary role in the formation of metric-to-decametric mounds and waterfalls, thus providing the required water supply and topographic potential.

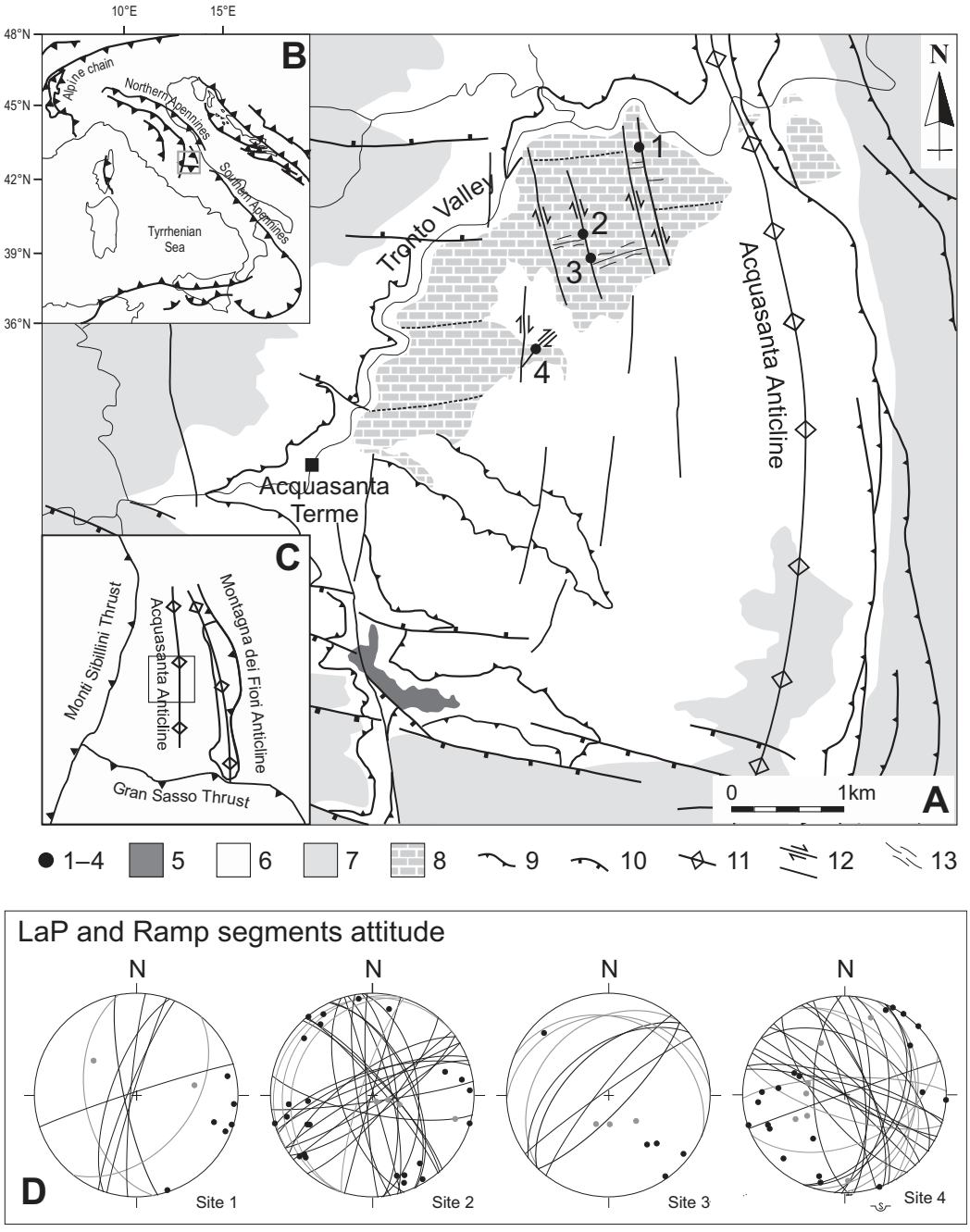

Figure 4. (A) Structural schematic map of the Acquasanta Terme area (modified from Menichetti, 2008). Legend: 1–4—location of the measure sites; 5—Scaglia Rossa Formation (Cretaceous–Paleocene); 6—Marly units, from Scaglia Variegata Formation to Marne a pteropodi Formation (Paleocene–Messinian); 7—Laga Formation (Messinian); 8—travertines; 9—thrust faults; 10—normal faults; 11—Acquasanta anticline hinge zone; 12—strike-slip faults (dotted when inferred); 13—fault-associated main fracture sets. (B) Tectonic sketch of the Italian region; inset shows location of C. (C) Tectonic setting of the Acquasanta area; inset shows location of A. (D) Stereoplots displaying the attitude of LaP (gray color) and ramp (black) segments measured outside fault zones for the various sites (Daisy software v3.54; Salvini et al., 1999). Dots represent poles to planes.

therein). The thrust-and-fold system progressively moved to the eastern sectors, as evidenced by the age of foredeep deposit migrations.

Active tectonic systems have been recognized in the foreland sector (offshore in the Adriatic Sea; e.g., Bigi et al., 1990; Scisciani and Calamita, 2009) and the outer front of the Northern Apennine (Caputo et al., 2012). Structural data, geophysical investigations, and focal mechanisms indicate that, at present, deformation is mainly accommodated along reverse faults fragmented by strike-slip and tear faults.

The Acquasanta Terme area is located in the southern sector of the Northern Apennines thrust-and-fold belt, which is characterized by a general NNW-SSE structural trend (Ogniben et al., 1975; Salvini and Vittori, 1982; Cavinato et al., 1986; Bigi et al., 1990, 1999; Scisciani et al., 2002; Di Francesco et al., 2010; Calamita et al., 2011).

Several interpretations are proposed in the literature for the mechanisms of development of the Apennine fold-and-thrust belt. According to Royden et al. (1987), the regional-scale deformation observed in the Apennines is controlled by deep segmentation of the lithosphere. Mattei et al. (1995) proposed the existence of combined clockwise and counterclockwise block rotation, resulting in strike-slip faulting during the Miocene–Pliocene chain development. According to Calamita et al. (2011), the present-day structural setting is influenced by the Triassic–Liassic extensional faults, which locally experienced inversion tectonics (Calamita et al., 2012; Pace and Calamita, 2013).

The studied travertine deposits are located between the main Monti Sibillini thrust front to the west and the Montagna dei Fiori anticline to the east (Fig. 4), and they lie on Oligocene–Miocene marls on the crest

of the thrust-related Acquasanta anticline. It is a N-S–striking, E-verging fold, ~20 km long, formed by the folded Mesozoic–Cenozoic carbonate succession (Koopman, 1983; Marsili and Tozzi, 1995), which represents the Ca-rich source for the travertine deposition (Menichetti, 2008).

The Acquasanta travertines are thermal-to-ambient water deposits of late Pleistocene age, developed on the SE side of the Tronto River Valley (Boni and Colacicchi, 1966; Farabollini et al., 2005). Three main travertine bodies associated with discontinuous depositional events are recognized, showing a trend of decreasing deposit volume and lowering elevation with time (Boni and Colacicchi, 1966; Ghisetti et al., 2001; Anzalone et al., 2013). These bodies include hydrothermal mounds, moderate to gentle slopes, waterfall-pool-dam and shallow lake-pond-marsh-swamp environments with a broad spectrum of low to high energy (Figs. 5, 6, and 7).

In this area, the Miocene structures are locally overprinted by a dextral strike-slip fault system striking N-S that involves also the Quaternary travertines of Acquasanta Terme (Menichetti, 2008; Boni and Colacicchi, 1966; Farabollini et al., 2005). E-W–striking fractures and normal faults also occur, associated with the strike-slip fault system.

STAIRCASE FRACTURES

Fracture Patterns in the Acquasanta Terme Travertines

In the Acquasanta Terme area, four quarries were examined both in the field and by picture analyses (sites 1–4, Fig. 4).

Sites 1 and 4 are characterized by hydrothermal mound deposits topped by shallow lake deposits (Fig. 5) and calcareous tufa deposits characterized by high porosity and macrophyta (Fig. 6). Sites 2 and 3 are characterized by gentle slope deposits showing prograding geometry and draped texture (Fig. 7).

Travertine brittle deformation, as evidenced from field observations, is characterized by a moderate fracturing with the presence of N-S–trending strike-slip faults that crosscut the whole travertine bodies (Figs. 5 and 6).

Fractures in the Acquasanta Terme quarries can be grouped into two classes: localized and scattered fracture systems (Figs. 5 and 6). Localized fracture systems are concentrated within the strike-slip fault damage zones and are characterized by fracture sets oriented according to the fault kinematics (i.e., Riedel planes sensu lato; Figs. 5B and 6C). Scattered fractures develop in the whole travertine deposit, without evident association to the main faults (Figs. 5C and 6B). Their attitude is typically affected by the geometry of the travertine body to form a characteristic staircase geometry, since their development is strongly influenced by the travertine internal laminations.

The resulting trajectory of scattered fractures shows an alternate double pattern (Figs. 2, 7, and 8). Depending on the geometrical relation between the internal laminations and the fracture surface portions, are distinguished fracture segments running parallel to the internal laminations or layering, in the following both referred as LaP, and fracture segments crosscutting it, in the following referred as ramps. Fracture trends following this (alternate) pattern have been named staircase fractures.

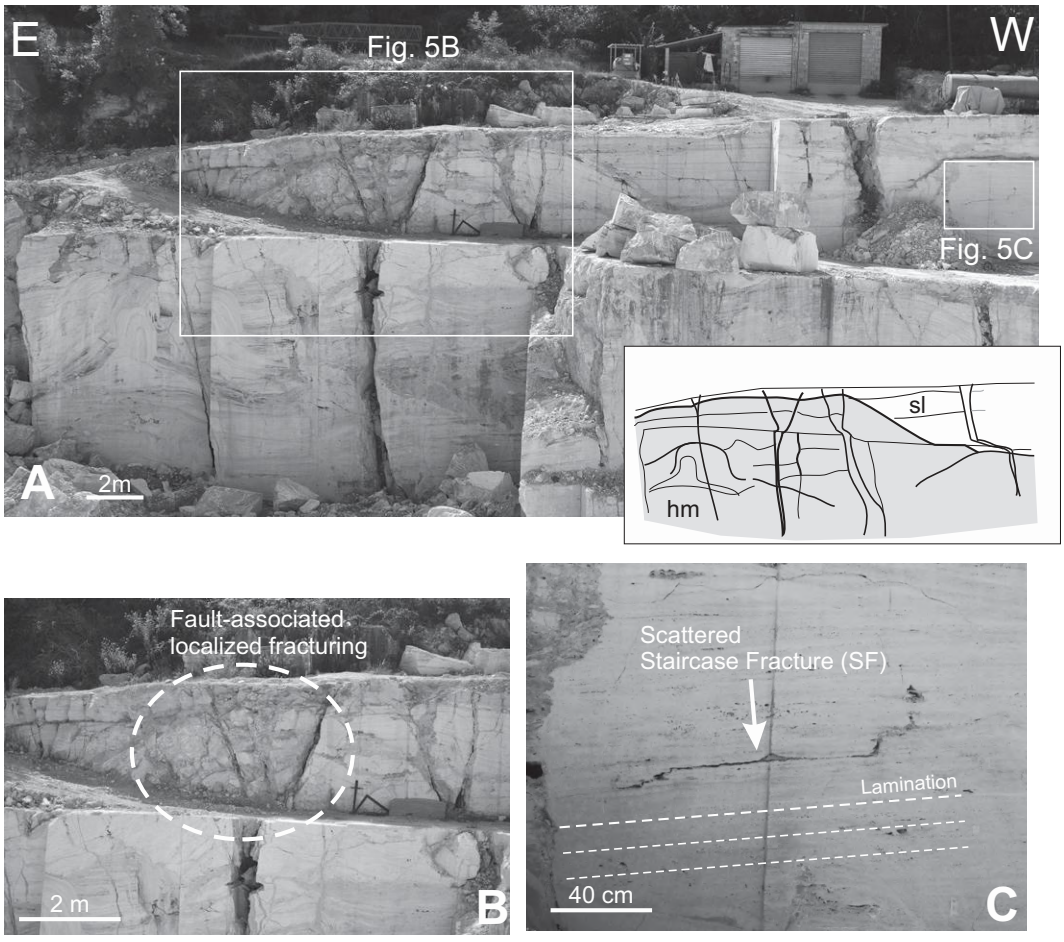

Figure 5. (A) Example of mound deposits (hm) evolving to shallow lake environment (sl). (B) One of the N-S–trending strike-slip faults crosscutting the mound deposits and inducing localized fracturing. These fractures were not considered in the present study. (C) Scattered fracture with staircase geometry in pond environment.

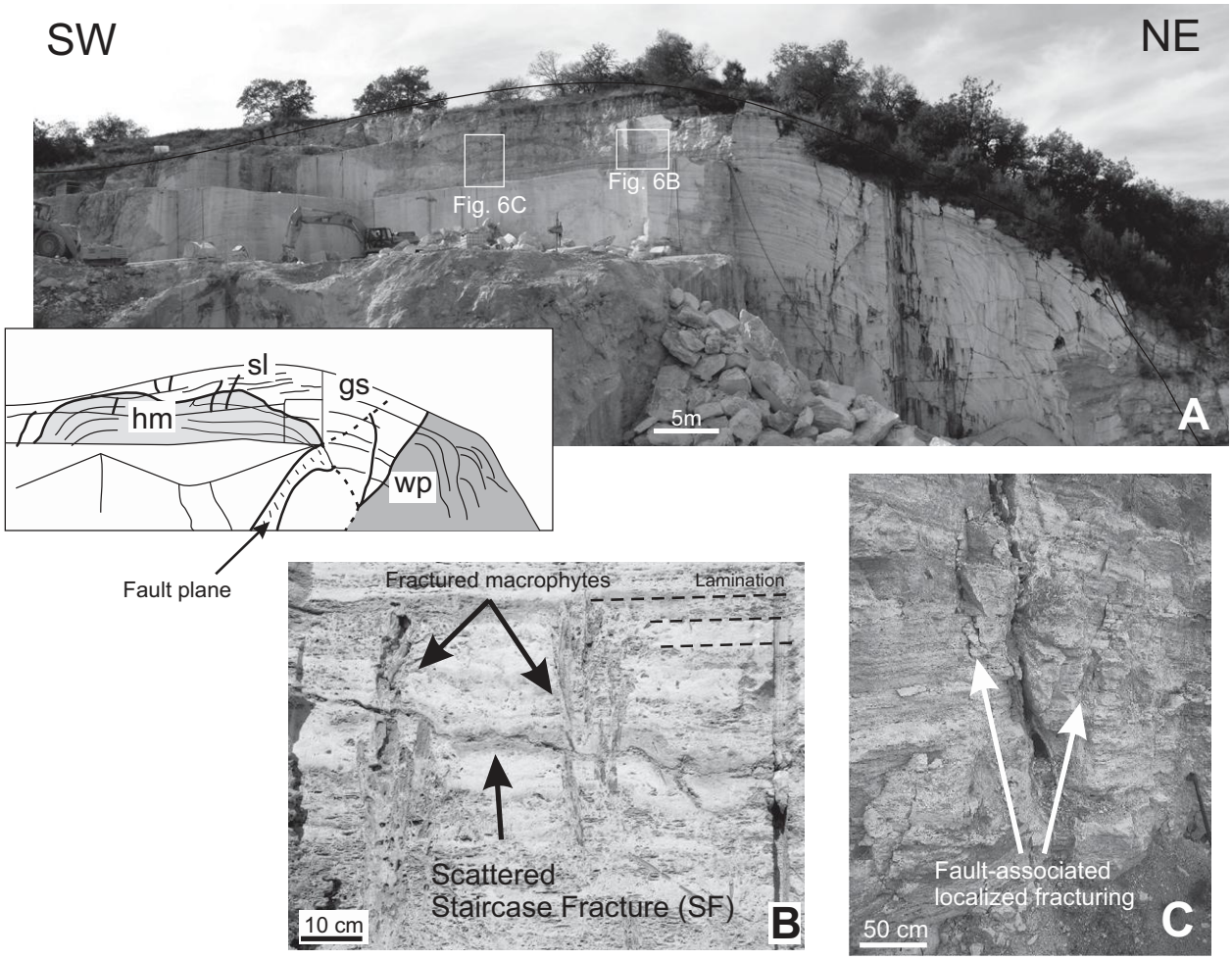

Figure 6. (A) Example of mound deposit (hm, bottom left) laterally evolving to gentle slope (gs) self-sustained waterfall (wp, right side) with swamp deposits (sl) on top. A fault termination crosscuts the outcrop wall in the waterfall zone. (B) Scattered fracture with staircase geometry in swamp environment. Macrophyta relics are displaced by the slip along the layer-parallel fractures. (C) Ridge-like structures along a fault and the associated fault-related fractures.

LaP localize along the porous layers or at the interface with tight laminae (Fig. 8A). Ramps cut both porous and tight laminae. As a result, not all porous laminae localize LaP, yet all LaP are localized along porous laminae. The scattered distribution of LaP and ramps azimuths (Fig. 4D) allows us to exclude a tectonic origin for this type of fracture in the Acquasanta Terme.

Ramps often show an extensional component, with a fracture opening of the order of millimeters, or more rarely of centimeters (Fig. 7). On the other hand, LaP often show a limited shear component (Fig. 7), locally expressed by the presence of a synthetic fracture cleavage that may eventually represent incipient staircase fracturing (Fig. 8A).

Staircase fractures are present at different outcrop scales, suggesting a rather scale-invariant distribution at the studied scale. Figure 8B shows a close-up of a mesoscale staircase fracture within a single porous level. On the other hand, as we will see, a critical volume is required to trigger the processes, thus limiting the self-similar geometry within a range of dimensions.

In most cases, the intersection geometry between ramps and LaP is very sharp with concordant dipping. The cutoff angles are the acute dihedral angles between the ramps and the lamination at the intersection (i.e., the corresponding LaP; Figs. 8 and 9), and they characterize the staircase geometry. In total, 69 LaP-ramp couples with their characteristic angle 216 and lengths were measured from 14 selected staircase fractures from the four different sites.

The LaP/Ramp Ratio (*L*/*R*)

The LaP/ramp (*L*/*R*) ratio is a dimensionless number that characterizes each fracture and is obtained by dividing the total length of LaP (*L*) by the total length of ramps (*R*). This parameter can be used to quantify the influence of the internal lamination on the fracture geometry. For a straight, lamination-independent fracture, *L* would be negligible, determining an *L*/*R* near to 0. The greater the *L*/*R* ratio, the stronger is the lamination influence on the fracture geometry. This *L*/*R* parameter allows us to group fractures into three families:

$L/R = 0$: the fracture geometry is independent of lamination (absence of LaP);
$0 < L/R \leq 1$: the fracture geometry is influenced by lamination (LaP are present but ramps are prevailing); and
$L/R > 1$: lamination rules the fracture geometry (LaP are prevailing).

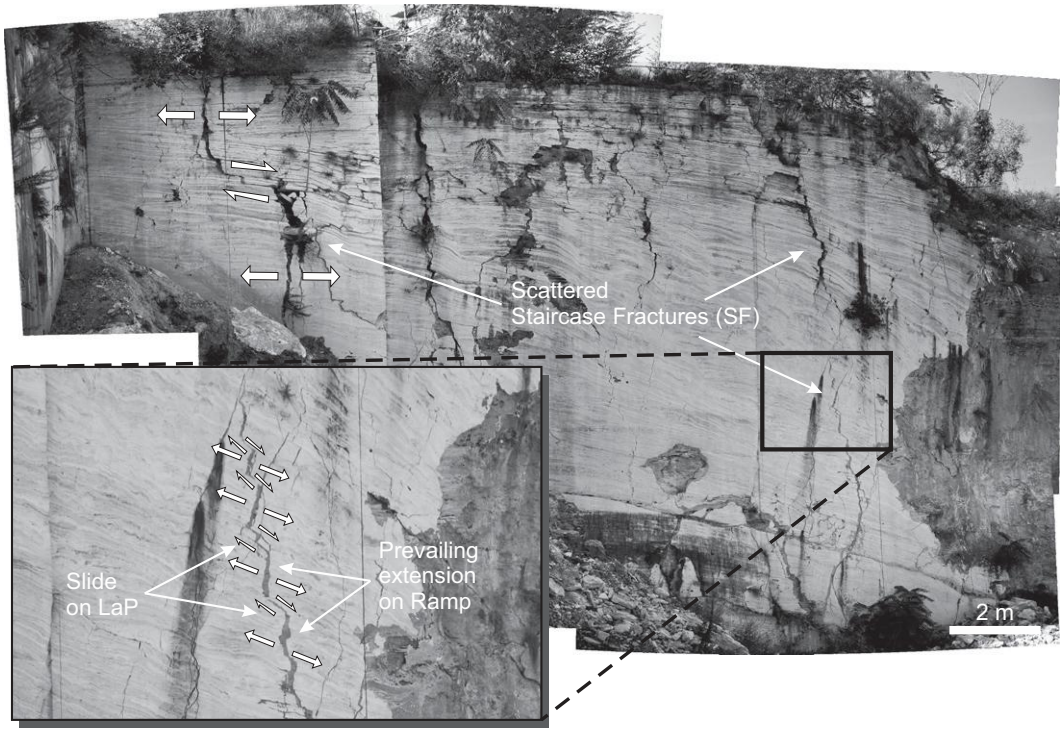

Figure 7. Examples of gentle slope deposits (gs). Scattered fractures with staircase geometry show prevailing extension in the ramps and sliding along the LaP.

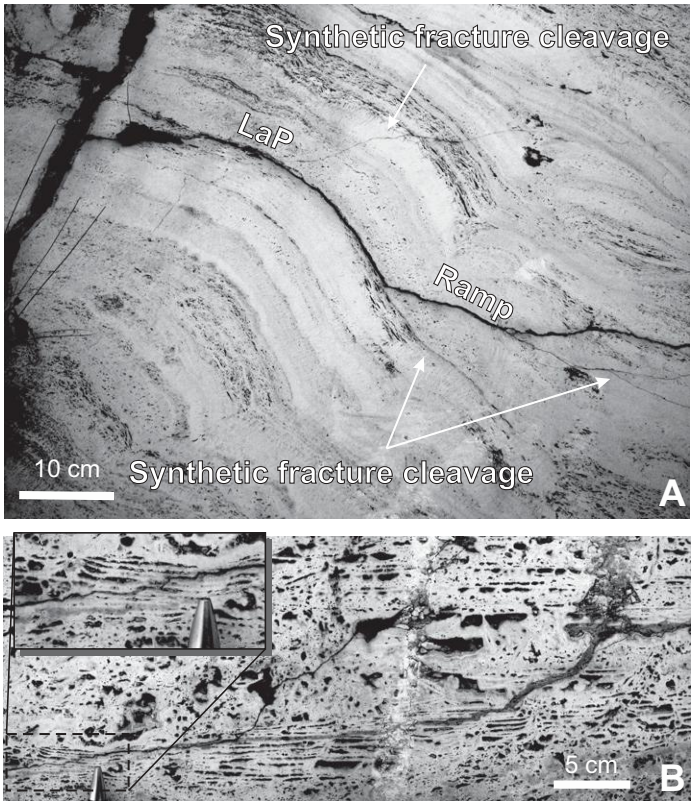

Figure 8. Examples of staircase fractures (SF). (A) Ramp crosscuts the lamination. LaP preferentially develop along the more porous level, resulting in the development of staircase fractures. (B) Enlarged-scale example of staircase fracture geometry.

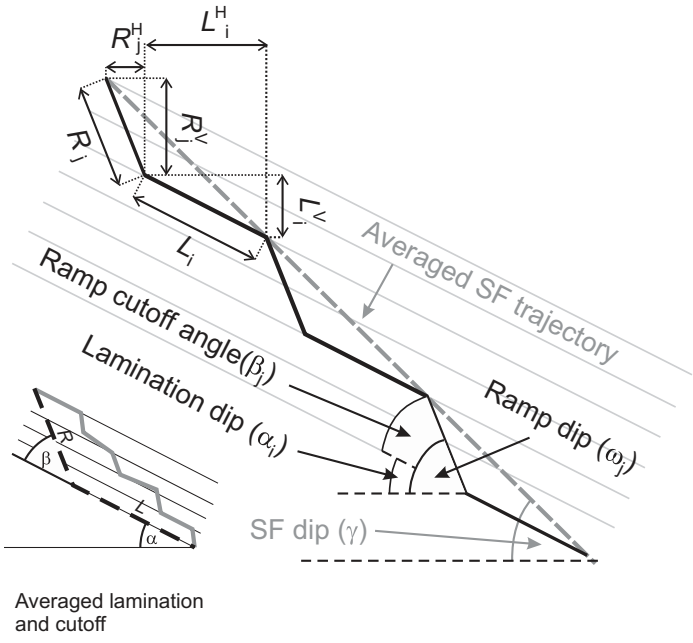

Figure 9. Schematic model of staircase fractures (SF). Each fracture is composed of a series of alternating LaP and ramp segments with a total length L and R, respectively. Ramps form a cutoff angle β with the lamination that has a dip of α. The averaged staircase fracture trajectory is described by the line joining the tips with a dip γ.

Data Collection

Measures of fracture attributes were collected from quarry wall pictures on optimally oriented vertical sections (i.e., orthogonal to the lamination-ramp intersection). This method is necessary to avoid bias in measuring segment lengths and attitudes by perspective, yet it strongly reduces the number of available fractures that can be properly measured.

To properly describe an entire quarry wall, a set of detailed, picture subsets was combined together using a dedicated software that includes a tool to partially correct the parallax error and optical distortions. Collected features for each fracture segment (LaP or ramp) include their length L_i and R_j, and the lamination dip α_i (Fig. 9), where i and j refer to the ith and jth LaP and ramp segments. Ramp features include also the cutoff angle β_j and the ramp dip ω_j. Length were measured by use of a reference dimension in the picture. The average lamination dip α for each fracture was obtained by a length weighted average of segment lamination dips. Similarly, the average cutoff angle β for each fracture was obtained by a length weighted average of ramp cutoff angles. The staircase fracture dip γ represents the averaged dip of a staircase fracture considering the dip of the ideal line connecting the two tips (Fig. 7). It can be measured directly from pictures (γ_M, measured) or computed (γ_C, computed) by projecting the LaP and ramps into their horizontal (H) and vertical (V) components according to the relation

$$\gamma = \arctan\left(\frac{\sum_{i=1}^{n} L_i^V + \sum_{j=1}^{m} R_j^V}{\sum_{i=1}^{n} L_i^H + \sum_{j=1}^{m} R_j^H}\right) = \arctan\left(\frac{\sum_{i=1}^{n}[L_i * \sin(\alpha_i)] + \sum_{j=1}^{m}[R_j * \sin(\omega_j)]}{\sum_{i=1}^{n}[L_i * \cos(\alpha_i)] + \sum_{j=1}^{m}[R_j * \cos(\omega_j)]}\right), \quad (1)$$

where n and m represent the number of LaP and ramp segments in each fracture, respectively; indexes V and H stand for vertical and horizontal components, and L_i and R_j represent the lengths of the ith and jth LaP and ramp segments, respectively.

Data Presentation

The fracture properties described in the methodology section (ratio between LaP and ramp total lengths, L/R; the average cutoff angle β; the staircase fracture dip γ) and the relative average lamination dip (α) are reported in Table 1. A careful examination was conducted to select the fractures with the proper characteristics for the purposes of the present paper, according to the previously described procedures.

Staircase fractures were collected in travertine deposits with α values ranging between 2° and 54°. Fracture total length (LaP + ramps) ranges between 0.2 and 8 m. L/R ranges between 0.08 and 5.05, with an average value of 1.43. The average cutoff angle β ranges between 35° and 70°, with an average value of 55.7°. The staircase fracture dip γ ranges between 10° and 78°, with an average value of 48.3°.

The staircase fracture dips γ_M and γ_C are presented in Table 1, as measured on the image and computed according to the aforementioned relations. The two methodologies provided similar results, with an average difference value of ~6°, indicating that the measured L/R ratios are representative of the staircase fracture geometry.

The measured and derived parameters were plotted as function of the average lamination dip α in the diagrams of Figure 10 to identify trends within the staircase fracture architecture with respect to the depositional

TABLE 1. STAIRCASE FRACTURE PROPERTIES

		LaP				Ramps					LaP + ramps					
		Total length (m)	n*	Average	St. dev	Total length (m)	m†	Average	St. dev	ω (°)	St. dev	Total length (m)	L/R	α (°)	β (°)	γ_M§ (°)	γ_C# (°)	$\Delta\gamma_{M-C}$ (°)
Flat zones	SiteD-2	1.17	2	0.58	0.29	0.46	2	0.15	0.14	46.33	16.04	1.63	2.54	2.57	44.67	21	15.56	5.44
	SiteD-3	4.00	5	0.80	0.63	0.79	4	0.20	0.07	54.75	18.84	4.80	5.05	2.60	51.75	10	9.75	0.25
	SiteA-3	1.84	2	0.61	0.76	0.67	3	0.17	0.10	62.75	25.58	2.52	2.74	5.88	59.50	20	19.87	0.13
	SiteC-5	0.12	7	0.01	0.01	0.08	8	0.01	0.01	44.44	18.18	0.20	1.39	8.58	35.11	23	18.19	4.81
	SiteA-2	1.66	3	0.33	0.19	1.07	3	0.21	0.15	43.20	10.28	2.73	1.56	11.10	34.60	24	21.58	2.42
	SiteC-4	1.69	9	0.19	0.25	2.57	9	0.29	0.35	71.78	13.01	4.26	0.66	11.13	70.33	56	47.23	8.77
	SiteA-4	1.01	3	0.34	0.04	1.68	3	0.24	0.17	59.00	18.93	2.69	0.60	17.75	62.86	43	38.74	4.26
	SiteC-3	1.75	7	0.19	0.19	3.08	8	0.28	0.32	83.36	5.35	4.84	0.57	22.49	62.91	66	63.92	2.08
	SiteA-1	0.28	4	0.14	0.02	3.61	4	0.60	0.39	50.00	17.15	3.89	0.08	24.60	75.83	69	44.52	24.48
	Mean	1.50				1.56				57.29		3.06	1.69		55.28	36.89	31.04	5.85
	St. dev.	1.13				1.25				13.54		1.54	1.56		14.76	22.08	18.22	7.50
Slope zones	SiteC-2	0.77	5	0.11	0.09	1.28	5	0.13	0.05	71.60	17.09	2.05	0.60	31.50	67.70	75	78.48	3.48
	SiteC-1	0.91	9	0.18	0.07	1.87	8	0.27	0.14	73.71	9.32	2.78	0.49	32.23	71.86	78	82.45	4.45
	SiteB-1	2.30	4	0.46	0.33	3.56	4	0.45	0.18	82.13	9.46	5.86	0.65	40.11	52.50	76	69.65	6.35
	SiteD-1	4.23	5	0.71	0.36	3.99	5	0.50	0.40	48.88	24.68	8.23	1.06	46.99	43.86	40	39.32	0.68
	SiteB-2	2.59	4	0.52	0.23	1.29	3	0.43	0.18	79.33	13.43	3.88	2.01	53.73	40.00	75	62.62	12.38
	Mean	2.16				2.40				71.13		4.56	0.96		55.18	68.80	66.50	5.47
	St. dev.	1.42				1.29				13.14		2.51	0.63		14.15	16.15	17.04	4.37
	Mean	1.68				1.80				58.88		3.43	1.45	22.23	52.72	45.94	41.32	5.83
	St. dev.	1.16				1.21				18.23		1.92	1.23	16.66	16.49	24.42	23.92	5.94

Note: LaP—lamination/layer-parallel fracture segment. Ramps—cross-cutting lamination fracture segments. α—average lamination dip. β—average cutoff angle. γ—staircase fracture dip.
*Number of LaP.
†Number of ramps.
§Measured.
#Calculated.

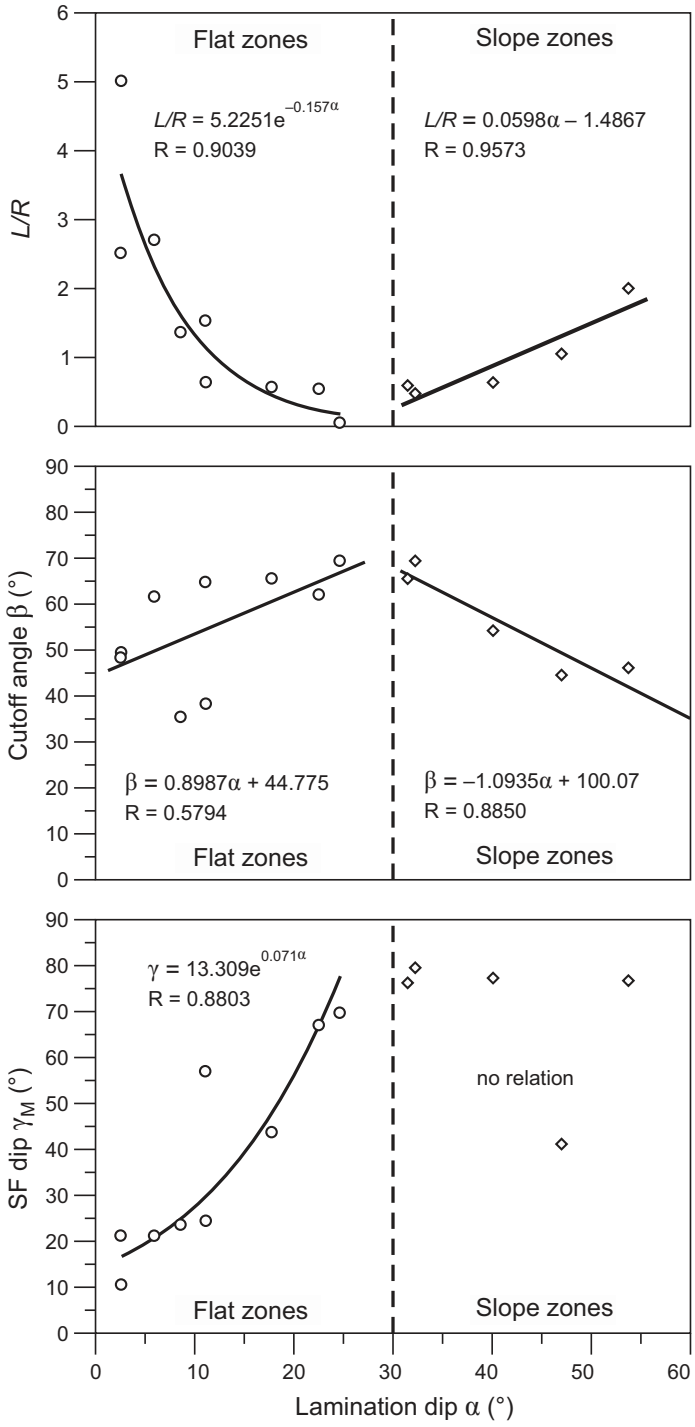

Figure 10. Empirical relations for *L/R* ratio, ramp cutoff angle (β), average ramp dip (γ), and lamination dip (α), for flat and slope zones, respectively. Lamination dip α around 30° marks a major change in the behavior of average staircase fracture angle, cutoff angle and *L/R* ratio. Apparently, no relation exists between α and γ in slope zones (α > 30°, right side), confirming that in these environments, the fracture dip is independent from the lamination dip. L—total length of LaP; R—total length of ramp fracture segments; SF—staircase fracture.

environments. The analyzed fracture characteristics include the *L/R* ratio, the average cutoff angle β, and the staircase fracture dip γ.

All diagrams are characterized by a dual behavior, with almost opposite trends separated by a discontinuity zone at a lamination dip around 30°. Based on these observations, two groups of staircase fractures can be defined: The first group relates to fractures developed in low-dipping laminations (α < 30°) and corresponds to low-energy-environment travertine deposits (shallow lake, pond, marsh, swamp; and moderate to gentle slope [gs]; Fig. 3). The second group relates to fractures developed in moderately to steeply dipping laminations (α > 30°) and corresponds to high-energy-environment deposits (hm and wp of Fig. 3).

In flat zones (α < 30°; Fig. 10), with increasing values of dip lamination, the empirical relations are as follows. (1) The *L/R* ratio shows decreasing values from 5 to nearly zero. The trend fits an exponential distribution with a negative exponent, and the best fit was achieved with the relation $L/R = 5.2251e^{-0.157\alpha}$. (2) The cutoff angle shows increasing values, fitting a linear trend where β = 0.8987α + 44.775. (3) The staircase fracture dip angle (γ) fits a positive exponential trend where $\gamma = 13.309e^{0.071\alpha}$.

In slopes zones (α > 30°; Fig. 10), with increasing values of dip lamination, the empirical relations are as follows. (1) *L/R* ratio linearly increases, and the best-fit trend is *L/R* = 0.598α –1.4876. (2) The cutoff angle linearly decreases, with β = –1.0935α + 100.07. (3) Staircase fracture dip angle shows almost constant values (with one outlier), suggesting no relation with the lamination dip angle (i.e., γ independent from α).

To summarize, our data show that low-energy flat-zone staircase fractures are characterized by: (1) higher *L/R* values (2–5), exponentially decaying with α; (2) scattered β values around 54°, related to the internal friction angle and the dimension of the sliding block (increasing by lowering β); and (3) subhorizontal to gently plunging staircase fracture dips (low γ), exponentially increasing with α. The staircase fracture dip γ might be considered representative of the strength of the rock, analogous to the other common fracture types. In this way, the found low γ and friction angle indicate a weak rock at the failure time. On the other hand, high-energy slope-zone staircase fractures are characterized by: (1) lower *L/R* values, linearly increasing with α; (2) β values linearly decreasing with α; and (3) an almost constant γ around 75°, independent from α.

DEVELOPMENT OF STAIRCASE FRACTURES BY GRAVITATIONAL SLIDING

Structural observations allow us to propose a model for staircase fracture formation in flat zones and slope zones. In particular, the measured parameters (namely the *L/R* ratio, the ramp segments total length *R*, the LaP total length *L*, the lamination dip α, and the cutoff angle β) were used to model the stress and strength conditions acting during staircase fracture formation.

The observed lamination dips are indicative of the sedimentary physical properties of the various depositional environments (Fig. 3). Unlithified/incoherent sedimentation, characteristic of low-energy hydraulic regimes, is stable only below a critical lamination dip. On the other hand, to achieve a steeply dipping lamination, lithification must occur as soon as the bacterial/chemical encrustations are deposited.

Gravitational instabilities associated with typical progradation and aggradation of travertine deposits outward from the resurgence zones have been previous recognized as a possible mechanism for the development of fractures with layer-parallel attitudes in other sedimentary environments (de Wet et al., 1999; Xianghua and Ming, 2002).

In this section, we will develop and numerically test this idea, on the basis of the conceptual model presented in Figure 11.

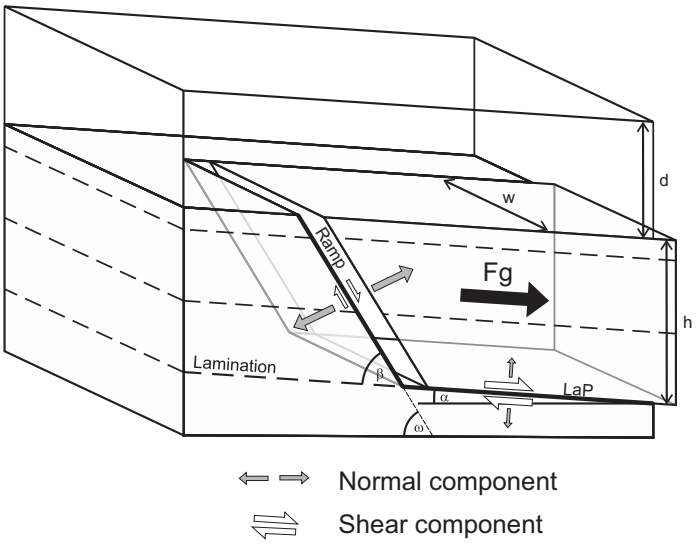

Figure 11. Conceptual model of staircase fracture geometry for the numerical modeling. The model consists of a couple of LaP and ramp surfaces. The relative dimensions of arrows are indicative of the intensity of the shear and normal components. Legend: *Fg*—gravity force sliding component; *h*—height; *w*—width; *d*—overburden; α—lamination dip; β—cutoff angle; ω—ramp dip.

Fracture Modeling

This model considers the dual and contrasting behavior observed in flat-zone (low energy, $\alpha < 30°$) and slope-zone (high energy, $\alpha > 30°$) staircase fracture parameters, suggesting a strong influence of the sedimentary physical properties of the various depositional environments in fracture development.

The geometry of staircase fractures was modeled by analytical modeling of the acting stress compared to the travertine strength during the failure (Salvini, 1993).

The model includes the contribution provided by the stresses related to the gravity sliding of the hanging wall and the overburden stress components acting on the failure surfaces. In order to avoid interferences with fault damage zones, fractures were collected sufficiently far from faulted zones.

The model consists of a hanging wall and a footwall separated by a couple of ramp and LaP fracture surfaces (Fig. 11). Fractures are modeled at their failure conditions, thus neglecting their successive displacements. The hanging wall has a half width *w* between the fault tips. An overburden of depth *d* is imposed over the fracture zone. Due to the encrustation nature of laminated travertine deposition, characterized by rather constant thicknesses, *d* was considered constant along the deposit.

The premise is that, at the inception of fracturing, forces due to gravity are in equilibrium with the forces generated by the strength along the staircase LaP and ramp surfaces

$$F_S = F_\Sigma^{LaP} + F_\Sigma^{Ramp}, \tag{2}$$

where F_S is the resulting gravity sliding force, F_Σ^{LaP} is the force produced by the strength (Σ) on the LaP surface, and F_Σ^{Ramp} is the force produced by the strength on the ramp surface. The fracture failure occurs when Equation 2 is satisfied.

The strength forces were calculated using the Coulomb failure criterion for the model geometry (see Appendix A for full analytical descriptions):

$$F_S = \rho g w \left\{ q R^2 \sin(\beta) + \frac{1}{2}\sin(\beta) R^2 \frac{\cos(\beta+\alpha)}{\cos(\alpha)} + d[R\cos(\beta+\alpha) + qR\cos(\alpha)] \right\} \cos(\alpha), \tag{3}$$

$$F_\Sigma^{LaP} = w\left\{ Lc^{LaP} + \tan(\varphi^{LaP})\frac{1}{3}L\rho g(R\sin(\beta)/\cos(\alpha) + d)[2+\cos(2\alpha)] - f_F \rho_W g\left[L(R\sin(\beta)/\cos(\alpha) + d) + \frac{1}{2}L^2\sin(\alpha)\right]\right\}, \tag{4}$$

$$F_\Sigma^{Ramp} = w\left\{ Rc^{Ramp} + \tan(\varphi^{Ramp})\frac{1}{3}R\rho g\left[d + \frac{1}{2}R\frac{\sin(\beta)}{\cos(\alpha)}\right][2+\cos(\beta+\alpha)] - f_F \rho_w g\left[Rd + \frac{1}{2}R^2\sin(\beta+\alpha)\right]\right\}, \tag{5}$$

where $\rho = 2500$ kg m^{-3} is the average rock density for Acquasanta travertines compatible with published values (Erdoğan, 2011), $g = 9.82$ m s^{-2} is the gravity acceleration, *w* is the fracture half width (m), *q* is the *L*/*R* ratio, *R* and *L* are the ramp and LaP across-strike length (m), respectively, β is the average ramp cutoff angle, α is the average lamination dip, *d* is the overburden thickness (m), c^{LaP} is the cohesion on the LaP surface (Pa), φ^{LaP} is the internal friction angle on the LaP surface, f_F is the fluid overpressure factor ($f_F = 0$, no fluid pressure; $f_F < 1$, drained fluid condition; $f_F \geq 1$ overpressure condition), $\rho_w = 1000$ kg m^{-3} is the water density, c^{Ramp} is the cohesion on the ramp surface (Pa), and φ^{Ramp} is the internal friction angle on the ramp surface. Please note that the width *w* is common to all three terms, implying that the found relation is independent of the width of the fracture *w*, which is therefore eliminated in the final equation. In this way the model can be reduced in an across-strike, two-dimensional section and LaP and ramp surfaces will be described by their corresponding lengths and angles.

Monte Carlo Modeling Results for Acquasanta Terme Laminated Rocks

Equation 2 was solved for flat-zone and slope-zone staircase fracture data to obtain the physical parameters at the fracture failure for the two environments. The solution was achieved by a Monte Carlo approach (Mosegaard and Tarantola, 2002; Tarantola, 2005).

The algorithm was tuned to generate 10^6 sets of random parameters, each ranging within a given interval, out of 10^{13} possible combinations. Each set of parameters was placed in the equations, and the root mean square (RMS) of the differences between the left and right terms was computed and associated similar to the deformation function (DF) approach (Storti et al., 1997). The solution is given by the set of parameters that provides the least RMS. The results provide the most reliable strength and stress conditions that will replicate the found geometry of all measured staircase fractures.

Several friction angles were tested and provided similar results, suggesting the independence of the model from this parameter. In this way, friction angle for both ramp and LaP was set to 30° for the final fitting. The output physical parameters generated by the Monte Carlo include the cohesion along ramps and LaP (c^{Ramp} and c^{LaP}, respectively), the overburden thickness (*d*), and the fluid overpressure fraction (f_F).

TABLE 2. RESULTS FROM MONTE CARLO ANALYSIS

Parameter	Flat zones	Slope zones	Monte Carlo solution drawing ranges	
			Min	Max
Cohesion ramp (Pa)	26,005	39,019	0	100,000
Cohesion layer-parallel (Pa)	19,107	37,826	0	100,000
Fluid overpressure	1.04	0.83	0	200
Overburden thickness (m)	1.14	4.55	0	10
Root mean square (RMS) (N)	2337	2905		

Values for the best fit are shown in Table 2. The final RMS values of 2337 N for flat zone and 2905 N for slope zone are reasonably low as compared with the average acting gravitational forces (around 200,000 N). Cohesion values are low in both flat zone and slope zone (<40,000 Pa; see Table 2), similar to what is suggested in literature for travertine tensile strength (Pentecost, 2005) and in compressive uniaxial tests (Erdoğan, 2011). In the slope zone, the cohesion is higher than the flat zone both in ramp (150%) and LaP (200%). Slight fluid overpressure (i.e., $f_F \geq 1$) is required only in the flat zone (1.04). On the other hand, 4.55 m of overburden thickness provided the ideal fracturing condition in the slope zone, while about 1 m (1.14 m) was required in the flat zone. The 1.14 m thickness is compatible with sediment thicknesses in lacustrine environments reported in the literature, ranging between 0.4 and 4 m (Wright, 2012).

These opposite trends are compatible with the different strengths of the rocks during staircase fracture formation.

According to our results, the development of LaP in the low-energy flat-zone staircase fracture suggests the presence of fluid overpressure (near-lithostatic) in poorly cemented sediments. These conditions can be easily achieved if these fractures develop in poorly cemented media during syndepositional or early diagenesis time, conditions which are likely to occur in swamp deposits.

On the other hand, slope-zone staircase fractures initially form as shear fractures, with a subordered extensional component that is added during movement (transtensional), in self-sustained/lithified media. The increasing *L*/*R* trend indicates that a significant component of the vertical stress produces a shear component along the lamination surfaces, which become more and more compatible sliding surfaces by increasing α.

The reliability of the solution is shown in the parameter frequency distributions of acceptable results (i.e., RMS < 6000 N) of the Monte Carlo modeling that were obtained during the processing (Fig. 12). Flat zones (flat zone; Figs. 12A–12D, histograms) are characterized by a skewed distribution and a general discordance between best-fit and modal values. A slight cohesion difference is observed between c^{Ramp} (19,000 Pa, more cohesive) and c^{LaP} (3667 Pa, almost incoherent), and this is more evident in the modal values. These values are compatible with tensile strength values obtained experimentally on microbial mats and soils (Nearing et al., 1991; Vignaga et al., 2012), suggesting that the initial fracturing conditions are likely to occur pre- and/or syn-diagenesis. The frequency of fluid overpressure factor solutions shows a skewed distribution around a mode of 1.23 (Fig. 12C), confirming the requirement for some overpressure to induce fracturing. The frequency distribution of overburden thickness has a mode of 0.40 m (Fig. 12D), which is consistent with the sedimentological environment of travertine deposition. In the slope zone, the frequency of acceptable values shows a rather symmetrical distribution, with mode very close to best-fit values (Figs. 12E–12H, histograms). Cohesion values are higher with respect to flat zones, and no marked strength contrast is

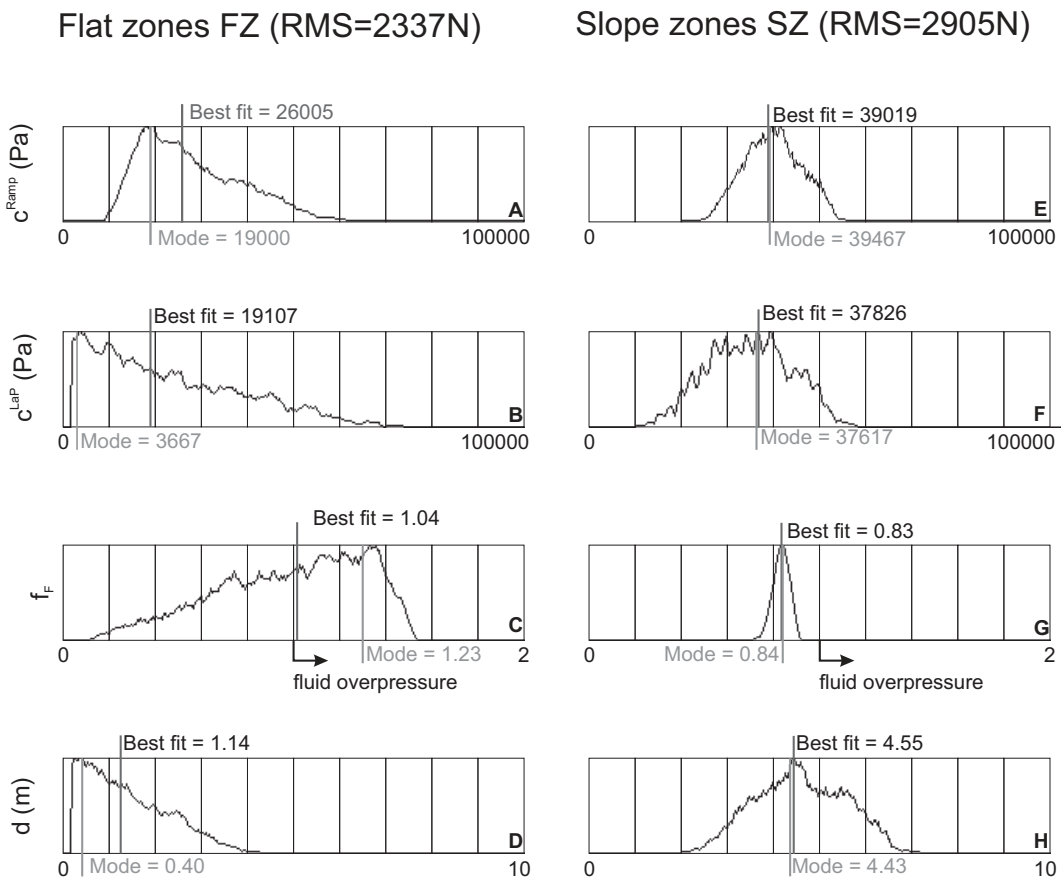

Figure 12. Acceptable solution (root mean square [RMS] < 6000 N) frequency histograms of modeled parameters for flat and slope zones. c^{Ramp} = ramp rock cohesion; c^{LaP} = lamination/layer-parallel rock cohesion; f_F = fluid overpressure factor; *d* = overburden. Solutions with $f_F > 1$ indicate fluid overpressure conditions. Fracturing occurs at very shallow depths (<1 m). The best fit does not always correspond to the more frequent solution values.

observed between ramps and LaP. The f_F values are always <1, indicating that fluid overpressure condition is never reached. On the other hand, a few meters of overburden (~5 m) are required for fracturing.

The correlation among the modeled parameters is shown in the probability scatterplots of Figure 13, showing the comparison between couples of parameters for both flat zones (Figs. 13A–13F, bottom-left sector) and slope zones (Figs. 13G–13L, upper-right sector). These diagrams show the distribution of acceptable solutions. A trend parallel to one of the two axes and a scattered distribution indicate the lack of correlation amongst the considered couple of parameters (e.g., Figs. 13G, 13H, and 13L).

In the flat zone, all parameters show a correlation. The relation between cohesion in LaP and ramps is confirmed (Fig. 13A). Fluid pressure plays an important role in reducing the cohesion-related strength of the rock, both in LaP and ramps (Figs. 13B–13C), and a relation with depth is also observed (Figs. 13D–13C). The values are strongly correlated with the depth. The cohesion to produce LaP is reduced to 0 at the surface (Fig. 13E).

In the slope zone (Figs. 13G–13L), a rather poor correlation between the cohesion in the LaP and in the ramps is present (Fig. 13G). The fluid pressure is not influencing the LaP and ramp cohesions (Figs. 13H and 13J), as well as depth (Fig. 13L), as evidenced by the near-vertical/horizontal trends in the scatterplots. As expected, by increasing depth, a higher cohesion is required on both LaP and ramps to form staircase fractures (Figs. 13I and 13K).

Key findings achieved with the Monte Carlo experiment on the staircase fracture model can be summarized as following: (1) a very low level of overpressure is necessary to develop staircase fractures in flat zones, and no overpressure is required in slope zones; (2) the overburden obtained in the experiment is quite consistent with environments where travertine deposits occur (~1 m in the flat zone; ~5 m in the slope zone); and (3) the higher cohesion obtained for slope zones is consistent with the higher cementation during deposition.

DISCUSSION

Fracturing in Self-Sustained versus Poorly Cemented Depositional Environments

The studied Acquasanta Terme travertine deposits are characterized by the presence of staircase fractures showing different degrees of textural control exerted by the travertine internal lamination/structuring, which in turn is dependent on the depositional environment. Results are summarized in the cartoon of Figure 14, where deposit geometry and sedimentary environment are compared with fracture architecture and fluid pore-pressure condition. In the studied examples, the main stress field is provided by the gravitational instability induced by the accumulation of travertine deposits, characterized by a variable lamination dip, and their tilting/sliding outward from the resurgence zone.

Staircase fractures in slope zones are those developed in higher-energy regimes (lamination dip > 30°, hydrothermal mound [hm] and waterfall-pool-dam [wp] environments; Fig. 3), where consolidated and strongly

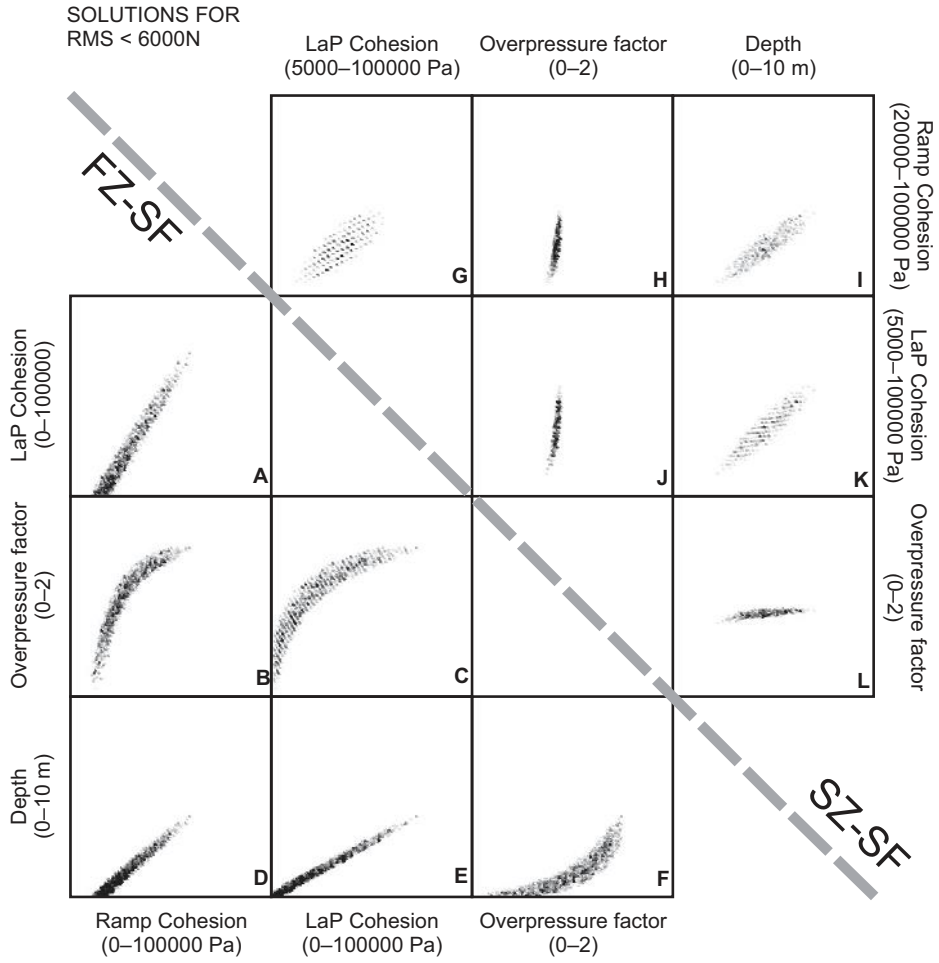

Figure 13. Probability density scatterplots between couples of parameters following Tarantola (2005). Dots represent couples of parameter values for solutions with root mean square (RMS) < 6000 N. Scatterplots are organized as a matrix with columns and rows corresponding to each parameter in covariance matrix style. (The parameters compared in each diagrams are reported on the left and bottom sides in flat zones [FZ] and right and top sides for slope zones [SZ].) These diagrams show the correlation between the couples of parameters obtained from the Monte Carlo fit for flat zone (A–F, bottom-left sector) and slope zone (G–L, upper-right sector) staircase fractures (SF). Oblique or curved trend of higher dot density shows the existing correlations. Trend parallel to the axes or scattered distributions indicate the independence of the considered couple of parameters. LaP—lamination-parallel fracture segment; FZ-SF—staircase fractures in flat zones; SZ-SF—staircase fractures in slope zones.

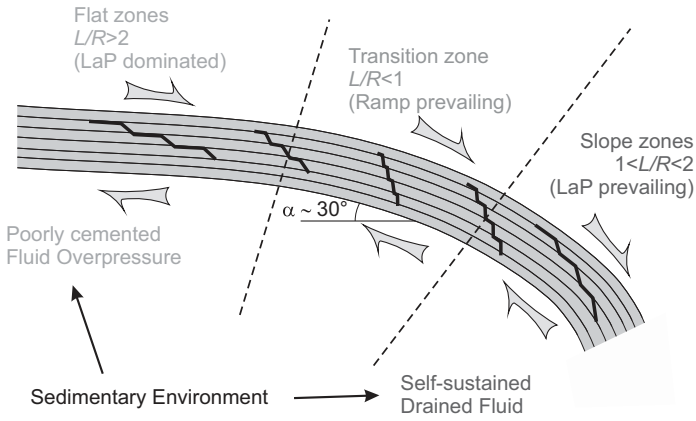

Figure 14. Schematic geological model for the development of staircase fractures and results achieved in our numerical modeling. The sketch represents the ideal distribution of staircase fractures in outcrops. The mechanical resistance (strength) is expected to be low in flat zones and high in slope zones. We speculate this could be explained by the intensity of diagenesis in the slope zones, where high dip lamination is self-sustained and where shear along lamination is favored. Overpressure is expected to occur in flat zones. LaP—lamination-parallel fracture segment; L—total length of LaP; R—total length of ramp fracture segments.

laminated travertines are deposited. In the slope zone, the increasing volume of travertines increases the loading, and the internal lamination is prone to sliding (Fig. 14). Staircase fractures in flat zones develop in subhorizontal laminated travertines, deposited in low-energy regimes (lamination dip < 30°, shallow lake or pond [sl] environment; Fig. 3), where poorly consolidated travertines are deposited. In this environment, the gravity sliding component is reduced, and staircase fractures are characterized by the highest values of *L*/*R* (>2 and up to 5), suggesting the primary role of lamination and fluid pore pressure in fracturing. The strong decrease in the *L*/*R* ratio by increasing α in the flat zone results from an increase of the gravity component along the LaP, thus requiring lower LaP length to achieve the failure conditions (Salvini, 1993; cf. Appendix A). The transition zone (lamination dip ~30°) easily relates to gentle slope environments (gs in Fig. 3). The formation of layer-parallel fractures (LaP in this paper) by gravity sliding has been proposed by de Wet et al. (1999), where the alternation of lithified microbialites and unconsolidated grainstone creates a differential response to gravity collapse.

Results from the Monte Carlo comparison show that there are two main factors controlling the architecture of fractures within microbialites: (1) resulting stress field (weight of the hanging wall block); and (2) the anisotropy of the mechanical properties produced by the sedimentary textures of the different depositional environments (including lamination, porosity, cohesion, and diagenesis).

These two factors combine, and the former prevails in slope-zone travertines. The latter is more evident in flat-zone travertines. An expression of the interference between the acting stress field and the internal anisotropy is represented by the found *L*/*R* values.

The role of fluid pressure has been recognized also in the formation of horizontal veins in mound environments (Gratier et al., 2012), and in a broader sense, fluid activity is one of the controlling factors in ruling the deformation style in the various tectonic settings and at different scales (Tenthorey et al., 2003; Jolivet et al., 2005; Cox, 2010; Putnis and Austrheim, 2010; Barnhoorn et al., 2010; Maggi et al., 2014). Within this condition, it is expected that local external stresses, such as seismic shaking, can trigger the development of staircase fracturing even in flat zones (Pratt, 1998; de Wet et al., 1999; Martín-Chivelet et al., 2011).

This model implies that the development of staircase fractures is a scale-dependent process, since a critical volume must be reached to induce sliding along the travertine internal structure. Nevertheless, after a minimum volume triggers the fracturing process, staircase fracture propagation at a smaller scale is present, influenced by the cyclic nature of travertine deposition.

Influence of Staircase Fracture Architecture on Permeability

Different from classical parallel fracture sets, staircase fractures provide higher intersection probability within the same fracture system, since a set of parallel staircase fractures may share LaP fracture segments. In this way, staircase fractures may potentially produce interconnected high-permeability pathways in microbial reservoirs (Fig. 3). Permeability is exponentially related to fracture aperture (Witherspoon et al., 1980), and rock elasticity relates the opening of fractures to their dimension (Olson, 2003). When ramps are bounded by a couple of LaP, their aperture is no longer limited by their length, thus providing more than the expected opening and higher-permeability pathways. The occurrence of staircase fractures in the Acquasanta Terme travertines is shown in Figure 15 and compared with a qualitative estimate of facies occurrence and average macroporosity. Combining these factors, it is possible to estimate the fracture-related permeability in the various environments. The highest fracture-related permeability is expected where staircase fractures are more frequent and/or the primary porosity is significant. Therefore, we infer that staircase fractures can potentially be a key element in addressing the permeability in swamps and shallow lake, gentle slope, and waterfall travertine environments (Figs. 14–15). Analogies between carbonate platforms and travertines (D'Argenio et al., 2008) allow us to extrapolate the relations found here to other microbialites environments, both continental and marine.

CONCLUSIONS

This study presents quantitative results on staircase fracture development, characteristic of poorly stratified yet strongly laminated microbialite/travertine sensu lato environments. In these rocks, lamination is provided by the alternation of tight and porous facies with different mechanical properties.

Staircase fractures may have a strong impact on fracture-related permeability given the connection of several porous laminae by a single fracture and the opening of ramp fractures apparently not limited by their length. A relation for depositional environment, staircase fracture occurrence, and enhanced permeability is proposed, suggesting shallow lake-marsh-pond, gentle slope, and waterfall as the more likely permeable environments.

The Acquasanta Terme studied staircase fractures developed in low-stress conditions (i.e., not induced by fault activity), and their geometry is mainly controlled by the travertine internal lamination. The observed and derived properties of staircase fractures (*L*/*R* ratio, cutoff angle, staircase fracture dip) relate to the average lamination dip and permit us to group staircase fractures in two families with opposite trends. In particular, the *L*/*R* factor (the ratio between lamination-parallel and ramp segment lengths) resulted in a useful parameter for quantifying the effect of lamination mechanical anisotropy on fracture architecture. For lamination dip steeper than 30°, the effect of the lamination increases with the lamination dip angle (higher *L*/*R* for steeply dipping laminated travertines). For lamination dip angles lower than 30°, the effect of the lamination increases as

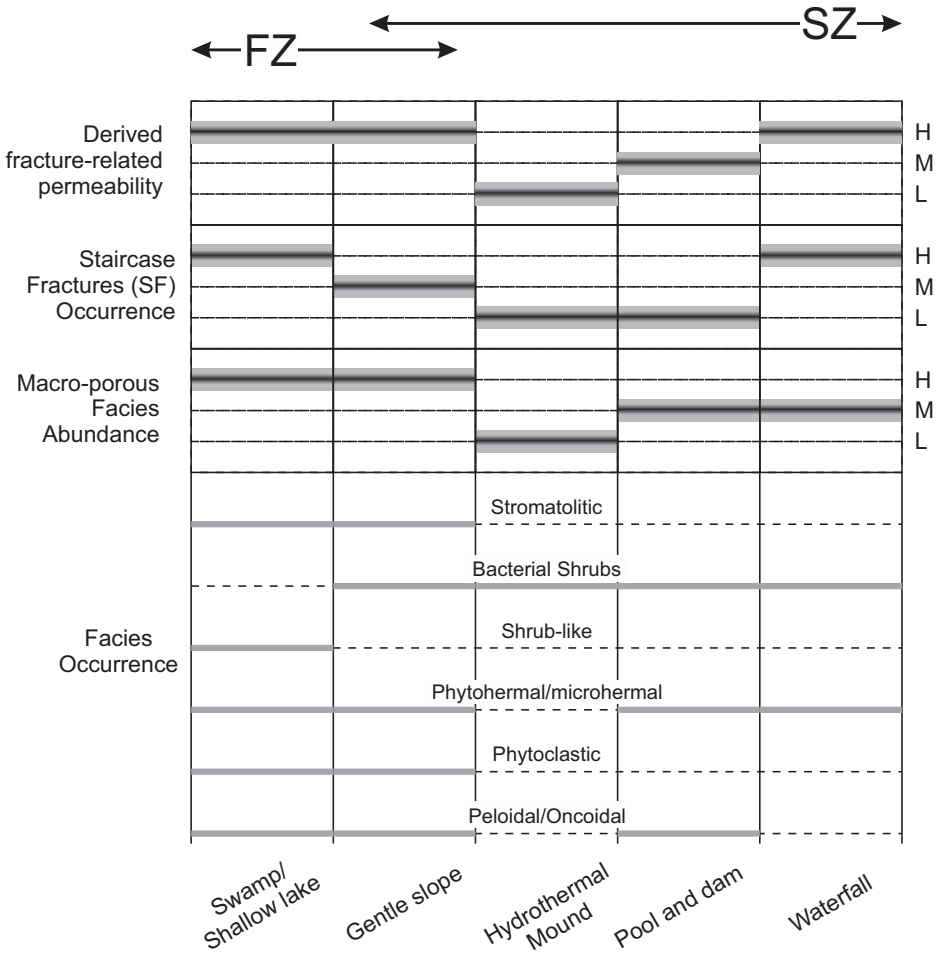

Figure 15. Synoptic table of expected fracture-related permeability in the various environments, according to our results. The facies occurrence in the various environments is synthetized from recent works on travertine deposits in central and southern Italy (Anzalone et al., 2007; Capezzuoli et al., 2008; Brogi et al., 2012). FZ—flat zones; SZ—slope zones; H—high; M—medium; L—low.

the lamination dip decreases (higher *L*/*R* for subhorizontally laminated travertines). We attribute this dual behavior to the physical sediment properties of high-energy slope zones (hydrothermal mound, pool and dam, and waterfall environments) compared to low-energy flat zones (shallow lake, marsh, pond, and swamp environments) in the thermal-to-freshwater travertine deposit of Acquasanta Terme.

In this framework, a genetic model is proposed involving gravity sliding as the trigger for staircase fracture formation. In slope zones, the steep lamination is prone to accommodate sliding inducing staircase fracturing. In flat zones, where the gravity component is reduced, poorly cemented sediments and fluid overpressure reduce friction, easing staircase fracturing.

We ran a Monte Carlo simulation to test the boundary conditions for the formation of staircase fractures by gravity sliding in flat zones and slope zones considering the strength contrasts between porous and tight levels, fluid overpressure, and the overburden conditions. Results from this analysis are satisfactory and confirm the proposed genetic model for staircase fractures. In this way, they represent a useful tool for the study of analogues for the evolution of porosity/permeability properties during deformation under low confining pressure, in hydrocarbon and geothermal fields.

APPENDIX A. COMPUTATION OF THE FORCE EQUILIBRIUM

The failure condition for the staircase fracturing model is achieved when the resistance forces are balanced by the acting force according to

$$F_S = F_\Sigma^{LaP} + F_\Sigma^{Ramp}, \tag{A1}$$

where F_S is the sliding force (i.e., the weight force component along the LaP surface), and F_Σ^{LaP} and F_Σ^{Ramp} are the strength forces (i.e., the forces produced by the shear strength along LaP and ramp surfaces, respectively). The sliding component along the LaP surface is computed according to

$$F_S = \rho g V \cos(\alpha), \tag{A2}$$

where ρ is the rock density (2500 m kg^{-3}), g is the gravity acceleration (9.82 m s^{-2}), V is the volume of the sliding block, and α is the average lamination dip (Fig. A1). The volume of the sliding block is computed as a prism that has the base coincident with the surface parallel to the maximum dip and height coincident with the width w. The calculation of the base is done by dividing it into three main subsurfaces (Fig. A1)

$$V = w(S1 + S2 + S3). \tag{A3}$$

In order to ease the computing of the subsurfaces, the following geometrical parameters are introduced:

$$j = R\frac{\cos(\beta + \alpha)}{\cos(\alpha)}, \tag{A4}$$

$$t = R\sin(\beta), \tag{A5}$$

$$k = t\tan(\alpha), \tag{A6}$$

$$h = t/\cos(\alpha), \tag{A7}$$

where R is the ramp across-strike length, and β is the average ramp cutoff angle. In addition, d is the thickness of the overburden, and L is the LaP across-strike length. The ramp dip ω is obtained from

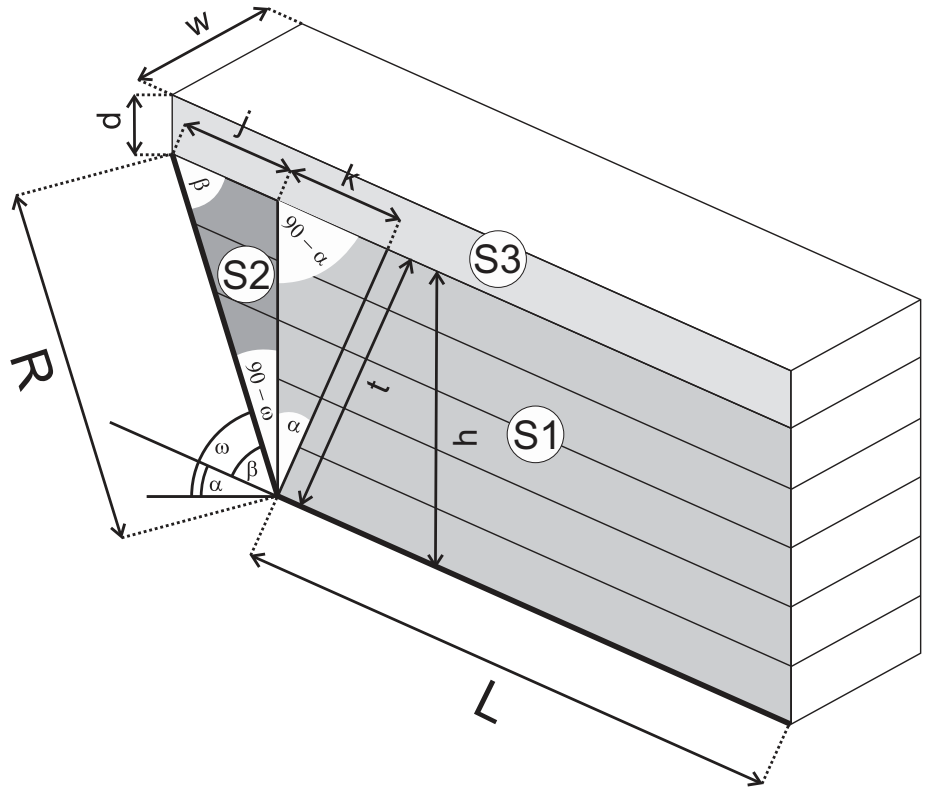

Figure A1. Surfaces and symbols used for the geometrical computation.

$$\omega = \beta + \alpha. \tag{A8}$$

The resulting surfaces for the three areas are:

$$S1 = Lt = LR\sin(\beta), \tag{A9}$$

$$S2 = \frac{1}{2} jt = \frac{1}{2}\sin(\beta) R^2 \frac{\cos(\beta+\alpha)}{\cos(\alpha)}, \tag{A10}$$

$$S3 = d[R\cos(\beta+\alpha) + L\cos(\alpha)]. \tag{A11}$$

Substituting the three surfaces in Equation A3, the volume is

$$V = w\left(LR\sin(\beta) + \frac{1}{2}\sin(\beta) R^2 \frac{\cos(\beta+\alpha)}{\cos(\alpha)} + d[R\cos(\beta+\alpha) + L\cos(\alpha)]\right). \tag{A12}$$

Combining Equations A2 and A12, the resulting equation for F_S is a function of w, L, R, β, and α:

$$F_S = \rho g w\left\{qR^2\sin(\beta) + \frac{1}{2}\sin(\beta) R^2 \frac{\cos(\beta+\alpha)}{\cos(\alpha)} + d[R\cos(\beta+\alpha) + qR\cos(\alpha)]\cos(\alpha)\right\}, \tag{A13}$$

where q is the L/R ratio. The strength forces on LaP and ramps are computed by integrating the effective strength on the relative surfaces

$$F_\Sigma^{LaP} = w\int_0^L \Sigma^{LaP} dl, \tag{A14}$$

$$F_\Sigma^{Ramp} = w\int_0^R \Sigma^{Ramp} dr, \tag{A15}$$

where F_Σ^{LaP} and F_Σ^{Ramp} are the strength forces, and Σ^{LaP} and Σ^{Ramp} are the strengths. The effective shear strengths are computed according to the Coulomb criterion

$$\Sigma^{LaP} = c^{LaP} + \tan(\varphi^{LaP})\Sigma_N^{LaP} - P_F^{LaP}, \tag{A16}$$

$$\Sigma^{Ramp} = c^{Ramp} + \tan(\varphi^{Ramp})\Sigma_N^{Ramp} - P_F^{Ramp}, \tag{A17}$$

where c^{LaP} and c^{Ramp} are the cohesions, φ^{LaP} and φ^{Ramp} are the internal friction angles, σ_N^{LaP} and σ_N^{Ramp} are the normal stress components, and P_F^{LaP} and P_F^{Ramp} are the fluid pore pressures. σ_N^{LaP} and σ_N^{Ramp} are solved using a two-dimension stress computation with the intermediate principal stress component parallel to the width direction (i.e., normal to the prism base)

$$\sigma_N^{LaP} = \frac{(\sigma_V^{LaP} + \sigma_H^{LaP})}{2} + \frac{\sigma_V^{LaP} - \sigma_H^{LaP}}{2}\cos(2\alpha), \tag{A18}$$

$$\sigma_N^{Ramp} = \frac{(\sigma_V^{Ramp} + \sigma_H^{Ramp})}{2} + \frac{\sigma_V^{Ramp} - \sigma_H^{Ramp}}{2}\cos(2\beta + 2\alpha). \tag{A19}$$

Here, σ_V^{LaP} and σ_V^{Ramp} are the vertical loads calculated along LaP and ramp surfaces, and σ_H^{LaP} and σ_H^{Ramp} are the relative horizontal components obtained by considering uniaxial stress conditions in an elastic medium and a Poisson ratio ν = 0.25.

$$\sigma_V^{LaP} = \rho g(h + d), \tag{A20}$$

$$\sigma_V^{Ramp} = \rho g\left(d + \frac{1}{2}h\right) = \rho g\left(d + \frac{1}{2}R\sin(\beta)/\cos(\alpha)\right), \tag{A21}$$

$$\sigma_H^{LaP} = \sigma_V^{LaP}\frac{\nu}{1-\nu} = \frac{1}{3}\sigma_V^{LaP}, \tag{A22}$$

$$\sigma_H^{Ramp} = \sigma_V^{Ramp}\frac{\nu}{1-\nu} = \frac{1}{3}\sigma_V^{Ramp}. \tag{A23}$$

Similarly, fluid pressure is computed by considering the height of the water table surface coincident with the top of the overburden,

$$P_F^{LaP} = f_F^{LaP}\rho_w g[h + d + L\sin(\alpha)], \quad \text{(A24)}$$

$$P_F^{Ramp} = f_F^{Ramp}\rho_w g[d + R\sin(\beta + \alpha)], \quad \text{(A25)}$$

where f_F^{LaP} and f_F^{Ramp} are the fractions of fluid overpressure along LaP and ramp surfaces ($f_F = 0$, no fluid pressure; $f_F < 1$, drained fluid condition; $f_F \geq 1$ overpressure condition). Combining Equations A14, A16, A18, A20, A22, and A24, we obtain the strength force relative to the LaP surface:

$$F_\Sigma^{LaP} = w\int_0^L \left\{ c^{LaP} + \tan(\omega^{LaP})\left[\frac{(\sigma_V^{LaP} + \sigma_H^{LaP})}{2} + \frac{\sigma_V^{LaP} - \sigma_H^{LaP}}{2}\cos(2\alpha)\right] - f_F^{LaP}\rho_w g[h + d + L\sin(\alpha)]\right\} dl. \quad \text{(A26)}$$

By solving the integral, we obtain

$$F_\Sigma^{LaP} = w\left\{ Lc^{LaP} + \tan(\omega^{LaP})\frac{1}{3}L\rho g(R\sin(\beta)/\cos(\alpha) + d)[2 + \cos(2\alpha)] - f_F^{LaP}\rho_w g\left[L(R\sin(\beta)/\cos(\alpha) + d) + \frac{1}{2}L^2\sin(\alpha)\right]\right\}. \quad \text{(A27)}$$

Combining Equations A15, A17, A19, A21, A23, and A25, we obtain the strength force relative to the ramp surface

$$F_\Sigma^{Ramp} = w\int_0^R \left\{ c^{Ramp} + \tan(\omega^{Ramp})\cdot\left[\frac{\sigma_{Vr}^{Ramp} + \sigma_{Hr}^{Ramp}}{2} + \frac{\sigma_{Vr}^{Ramp} - \sigma_{Hr}^{Ramp}}{2}\cos(2\beta + 2\alpha)\right] - f_F^{Ramp}\rho_w g[d + R\sin(\beta + \alpha)]\right\} dr, \quad \text{(A28)}$$

and solving the integral, we obtain

$$F_\Sigma^{Ramp} + w\left\{ Rc^{Ramp} = \tan(\omega^{Ramp})\frac{1}{3}R\rho g\left[d + \frac{1}{2}R\frac{\sin(\beta)}{\cos(\alpha)}\right]\cdot[2 + \cos 2(\beta + \alpha)] - f_F^{Ramp}\rho_w g\left[Rd + \frac{1}{2}R^2\sin(\beta + \alpha)\right]\right\}. \quad \text{(A29)}$$

ACKNOWLEDGMENTS

We are grateful to B. D'Argenio and E. Anzalone for having introduced us to travertines and the Acquasanta Terme outcrops, to L. De Filippis for support in the field, and to A. Gandin for further interesting discussions. E. Tavarnelli, F. Calamita, and M. Menichetti provided useful revisions. The quarry administrators of Acquasanta Terme, C. Allevi and G. Cappotti (La Fornara quarry), L. Cardi and A. Cardi (Marmi Cardi quarry), F. Tancredi (Fratelli Tancredi quarry), A. Amatizi (San Pietro quarry), and Tivoli Terme G. Squeo (Travertini Caucci quarry), are also thanked for their kindness and helpfulness. We acknowledge Petrobras for supporting the research and allowing the publication of this paper. M. Maggi dedicates this work to the loving memory of Alberto Spina.

REFERENCES CITED

Ahr, W.M., 2008, Geology of Carbonate Reservoirs. Hoboken, New Jersey, John Wiley & Sons, Inc., 296 p.

Ahr, W.M., 2009, Microbial carbonates as hydrocarbon reservoirs, *in* American Association of Petroleum Geologists convention. Denver, Colorado, American Association of Petroleum Geologists.

Amato, V., Anzalone, E., Aucelli, P.P.C., D'Argenio, B., Ferreri, V., and Rosskopf, C.M., 2012, Sedimentology and depositional history of the travertines outcropping in the Poseidonia-Paestum archaeological area. Rendiconti Lincei, v. 23, p. 61–68, doi:10.1007/s12210-011-0155-z.

Anzalone, E., 2008, Late Pleistocene travertines and their analogues under-deposition. A comparative analysis. Italian Journal of Quaternary Sciences, v. 21, p. 91–98.

Anzalone, E., Ferreri, V., Sprovieri, M., and D'Argenio, B., 2007, Travertines as hydrologic archives: The case of the Pontecagnano deposits (southern Italy). Advances in Water Resources, v. 30, p. 2159–2175, doi:10.1016/j.advwatres.2006.09.008.

Anzalone, E., Ferreri, V., and D'Argenio, B., 2013, I travertini pleistocenici di Acquasanta nelle Marche: Un modello di deposito da acque termali su versanti acclivi, *in* L'Associazione Italiana per lo Studio del Quaternario (AIQUA). Napoli, Italy, AIQUA, v. 19, p. 38.

Ascione, A., Iannace, A., Imbriale, P., Santangelo, N., and Santo, A., 2013, Tufa and travertines of southern Italy: Deep-seated, fault-related CO_2 as the key control in precipitation. Terra Nova, v. 26, p. 1–13, doi:10.1111/ter.12059.

Barbier, M., Hamon, Y., Callot, J.-P., Floquet, M., and Daniel, J.-M., 2012, Sedimentary and diagenetic controls on the multiscale fracturing pattern of a carbonate reservoir: The Madison Formation (Sheep Mountain, Wyoming, USA). Marine and Petroleum Geology, v. 29, p. 50–67, doi:10.1016/j.marpetgeo.2011.08.009.

Barnhoorn, A., Cox, S.F., Robinson, D.J., and Senden, T., 2010, Stress- and fluid-driven failure during fracture array growth: Implications for coupled deformation and fluid flow in the crust. Geology, v. 38, p. 779–782, doi:10.1130/G31010.1.

Becker, A., and Gross, M.R., 1996, Mechanism for joint saturation in mechanically layered rocks: An example from southern Israel. Tectonophysics, v. 257, p. 223–237, doi:10.1016/0040-1951(95)00142-5.

Bigi, G., Castellarin, A., Catalano, R., Coli, M., Cosentino, D., Dal Piaz, G.V., Lentini, F., Parotto, M., Patacca, E., Praturlon, A., Salvini, F., Sartori, R., Scandone, P., and Vai, G.B., 1990, Synthetic Structural-Kinematic Map of Italy, *in* Bigi, G., Cosentino, D., Parotto, M., Sartori, R., and Scandone, P., eds., Structural Model of Italy: Roma, Italy, Quaderni de "La Ricerca Scientifica del C.N.R. (Consiglio Nazionale delle Ricerche), scale 1:2,000,000.

Bigi, S., Calamita, F., Cello, G., Centamore, E., Deiana, G., Paltrinieri, W., Pierantoni, P.P., and Ridolfi, M., 1999, Tectonics and sedimentation within a Messinian foredeep in the Central Apennines, Italy. Journal of Petroleum Geology, v. 22, p. 5–18, doi:10.1111/j.1747-5457.1999.tb00456.x.

Boccaletti, M., Calamita, F., Deiana, G., Gelati, R., Massari, F., Moratti, G., and Ricci Lucchi, F., 1990, Migrating foredeep-thrust belt systems in the Northern Apennines and southern Alps. Palaeogeography, Palaeoclimatology, Palaeoecology, v. 77, p. 3–14, doi:10.1016/0031-0182(90)90095-O.

Boni, C., and Colacicchi, R., 1966, I travertini della valle del Tronto. Memorie della Societa Geologica Italiana, v. 5, p. 315–339.

Brogi, A., Capezzuoli, E., Buracchi, E., and Branca, M., 2012, Tectonic control on travertine and calcareous tufa deposition in a low-temperature geothermal system (Sarteano, central Italy). Journal of the Geological Society of London, v. 169, p. 461–476, doi:10.1144/0016-76492011-137.

Calamita, F., Satolli, S., Scisciani, V., Esestime, P., and Pace, P., 2011, Contrasting styles of fault reactivation in curved orogenic belts: Examples from the central Apennines (Italy). Geological Society of America Bulletin, v. 123, p. 1097–1111, doi:10.1130/B30276.1.

Calamita, F., Pace, P., and Satolli, S., 2012, Coexistence of fault-propagation and fault-bend folding in curve-shaped foreland fold-and-thrust belts: Examples from the Northern Apennines (Italy). Terra Nova, v. 24, p. 396–406, doi:10.1111/j.1365-3121.2012.01079.x.

Capezzuoli, E., Gandin, A., and Sandrelli, F., 2008, Evidence of associated deposition of travertine and calcareous tufa in the Quaternary carbonates of Valdelsa basin (Tuscany). Italian Journal of Quaternary Science, v. 21, p. 113–124.

Caputo, R., Iordanidou, K., Minarelli, L., Papathanassiou, G., Poli, M.E., Rapti-Caputo, D., Sboras, S., Stefani, M., and Zanferrari, A., 2012, Geological evidence of pre-2012 seismic events, Emilia-Romagna, Italy. Annals of Geophysics, v. 55, p. 743–749, doi:10.4401/ag-6148.

Carmignani, L., Decandia, F.A., Disperati, L., Fantoui, P.L., Lauarotto, A., and Oggiano, G., 1995, Relationships between the Tertiary structural evolution of the Sardinia-Corsica-Provencal Domain and the Northern Apennines. Terra Nova, v. 7, p. 128–137, doi:10.1111/j.1365-3121.1995.tb00681.x.

Carminatti, M., Wolff, B., and Gamboa, L., 2008, New exploratory frontiers in Brazil, *in* 19th World Petroleum Congress. Madrid, Spain.

Cavinato, G.P., Salvini, F., and Tozzi, M., 1986, Evoluzione strutturale del settore centrale della linea Olevano-Antrodoco. Memorie della Società Geologica Italiana, v. 35, p. 591–601.

Chafetz, H., and Folk, R., 1984, Travertines: Depositional morphology and the bacterially constructed constituents. Journal of Sedimentary Research, v. 54, p. 289–316.

Cianfarra, P., and Salvini, F., 2014, Lineament domain of regional strike-slip corridor: Insight from the Neogene transtensional De Geer transform fault in NW Spitsbergen. Pure and Applied Geophysics, doi:10.1007/s00024-014-0869-9.

Ciarapica, G., and Passeri, L., 2002, The paleogeographic duplicity of the Apennines. Bollettino della Società Geologica Italiana, v. 121, no. 1, p. 67–75.

Cooke, M.L., Simo, J.A., Underwood, C.A., and Rijken, P., 2006, Mechanical stratigraphic controls on fracture patterns within carbonates and implications for groundwater flow. Sedimentary Geology, v. 184, p. 225–239, doi:10.1016/j.sedgeo.2005.11.004.

Cox, S.F., 2010, The application of failure mode diagrams for exploring the roles of fluid pressure and stress states in controlling styles of fracture-controlled permeability enhancement in faults and shear zones. Geofluids, v. 10, p. 217–233, doi:10.1111/j.1468-8123.2010.00281.x.

D'Argenio, B., 2001, From megabanks to travertines—The independence of carbonate rock growth-forms from scale and organismal templates through time, *in* Guerzoni, S., Harding, S., Lenton, T., and Ricci-Lucchi, F., eds., Earth System Science: Proceedings of the International School of Earth and Planetary Sciences. Siena, Italy, International School of Earth and Planetary Sciences, p. 109–130.

D'Argenio, B., and Ferreri, V., 2004, Travertines as self regulating carbonate systems. Evolutionary trends and classification. Földtani Közlöny, v. 1343, p. 209–218.

D'Argenio, B., Ferreri, V., and Anzalone, E., 2008, Travertines and carbonate platforms. Geometries and evolutionary trend. Rendiconti della Società Geologica Italiana, v. 2, p. 67–72.

De Filippis, L., Faccenna, C., Billi, A., Anzalone, E., Brilli, M., Ozkul, M., Soligo, M., Tuccimei, P., and Villa, I.M., 2012, Growth of fissure ridge travertines from geothermal

springs of Denizli Basin, western Turkey. Geological Society of America Bulletin, v. 124, p. 1629–1645, doi:10.1130/B30606.1.

De Filippis, L., Faccenna, C., Billi, A., Anzalone, E., Brilli, M., Soligo, M., and Tuccimei, P., 2013a, Plateau versus fissure ridge travertines from Quaternary geothermal springs of Italy and Turkey: Interactions and feedbacks between fluid discharge, paleoclimate, and tectonics. Earth-Science Reviews, v. 123, p. 35–52, doi:10.1016/j.earscirev.2013.04.004.

De Filippis, L., Anzalone, E., Billi, A., Faccenna, C., Poncia, P.P., and Sella, P., 2013b, The origin and growth of a recently-active fissure ridge travertine over a seismic fault, Tivoli, Italy. Geomorphology, v. 195, p. 13–26, doi:10.1016/j.geomorph.2013.04.019.

de Wet, C.B., Dickson, J.A.D., Wood, R.A., Gaswirth, S.B., and Frey, H.M., 1999, A new type of shelf margin deposit: Rigid microbial sheets and unconsolidated grainstones riddled with meter-scale cavities. Sedimentary Geology, v. 128, p. 13–21, doi:10.1016/S0037-0738(99)00055-X.

Dias, J.L., 2005, Tectonica, estratigrafia e sedimentacao no Andar Aptiano da margem leste brasileira. Boletim de Geociencias da Petrobras, v. 13, p. 7–25.

Di Francesco, L., Fabbi, S., Santantonio, M., Bigi, S., and Poblet, J., 2010, Contribution of different kinematic models and a complex Jurassic stratigraphy in the construction of a forward model for the Montagna dei Fiori fault-related fold (central Apennines, Italy). Geological Journal, v. 45, p. 489–505, doi:10.1002/gj.1191.

Di Naccio, D., Boncio, P., Cirilli, S., Casaglia, F., Morettini, E., Lavecchia, G., and Brozzetti, F., 2005, Role of mechanical stratigraphy on fracture development in carbonate reservoirs: Insights from outcropping shallow water carbonates in the Umbria–Marche Apennines, Italy. Journal of Volcanology and Geothermal Research, v. 148, p. 98–115, doi:10.1016/j.jvolgeores.2005.03.016.

Eisenstadt, G., and De Paor, D.G., 1987, Alternative model of thrust-fault propagation. Geology, v. 15, p. 630–633, doi:10.1130/0091-7613(1987)15<630.

Erdoğan, Y., 2011, Engineering properties of Turkish travertines. Scientific Research and Essays, v. 6, p. 4551–4566.

Faccenna, C., Soligo, M., Billi, A., De Filippis, L., Funiciello, R., Rossetti, C., and Tuccimei, P., 2008, Late Pleistocene depositional cycles of the Lapis Tiburtinus travertine (Tivoli, central Italy): Possible influence of climate and fault activity. Global and Planetary Change, v. 63, p. 299–308, doi:10.1016/j.gloplacha.2008.06.006.

Farabollini, P., Gentili, B., Materazzi, M., and Pambianchi, G., 2005, Freshwater travertines in central Apennine (Italy): Genesis and climatic and neotectonic significance. Revista de Geomorfologie, v. 7, p. 61–75.

Flügel, E., 2004, Microfacies of Carbonate Rocks: Analysis, Interpretation and Application. Berlin, Springer, 984 p.

Ford, T.D., and Pedley, H.M., 1996, A review of tufa and travertine deposits of the world. Earth-Science Reviews, v. 41, p. 117–175, doi:10.1016/S0012-8252(96)00030-X.

Fouke, B.W., Farmer, J.D., Des Marais, D.J., Pratt, L., Sturchio, N.C., Burns, P.C., and Discipulo, M.K., 2000, Depositional facies and aqueous-solid geochemistry of travertine-depositing hot springs (Angel Terrace, Mammoth Hot Springs, Yellowstone National Park, U.S.A.). Journal of Sedimentary Research, v. 70, p. 565–585, doi:10.1306/2DC40929-0E47-11D7-8643000102C1865D.

Fouke, B.W., Bonheyo, G.T., Sanzenbacher, B., and Frias-Lopez, J., 2003, Partitioning of bacterial communities between travertine depositional facies at Mammoth Hot Springs, Yellowstone National Park, USA. Canadian Journal of Earth Sciences, v. 40, p. 1531–1548, doi:10.1139/e03-067.

Fusari, A., Invernizzi, C., Pierantoni, P.P., and Carroll, M., 2013, Preliminary insights from the Acquasanta thermal area (Marche, Italy), *in* European Geothermal Congress. Pisa, Italy.

Galdenzi, S., Cocchioni, F., Filipponi, G., Morichetti, L., Scuri, S., Selvaggio, R., and Cocchioni, M., 2010, The sulfidic thermal caves of Acquasanta Terme (central Italy). Journal of Caves and Karst Studies, v. 72, p. 43–58, doi:10.4311/jcks2008es0056.

Gandin, A., Capezzuoli, E., Scienze, D., Siena, U., and Laterina, V., 2008, Travertine versus calcareous tufa: Distinctive petrologic features and stable isotopes signatures. Italian Journal of Quaternary Sciences, v. 21, p. 2008.

Ghisetti, F., Kirschner, D.L., Vezzani, L., and Agosta, F., 2001, Stable isotope evidence for contrasting paleofluid circulation in thrust faults and normal faults of the central Apennines, Italy. Journal of Geophysical Research, v. 106, p. 8811–8825, doi:10.1029/2000JB900377.

Golubić, S., Violante, C., Plenković-Moraj, A., and Grgasović, T., 2008, Travertines and calcareous tufa deposits: An insight into diagenesis. Geologia Croatica, v. 61, p. 363–378.

Gratier, J.P., Frery, E., Deschamps, P., Royne, A., Renard, F., Dysthe, D., Ellouz-Zimmerman, N., and Hamelin, B., 2012, How travertine veins grow from top to bottom and lift the rocks above them: The effect of crystallization force. Geology, v. 40, p. 1015–1018, doi:10.1130/G33286.1.

Gross, M., and Eyal, Y., 2007, Throughgoing fractures in layered carbonate rocks. Geological Society of America Bulletin, v. 119, p. 1387–1404, doi:10.1130/0016-7606(2007)119[1387:TFILCR]2.0.CO;2.

Hancock, P.L., Chalmers, R.M.L., Altunel, E., and Çakir, Z., 1999, Travitonics: Using travertines in active fault studies. Journal of Structural Geology, v. 21, p. 903–916, doi:10.1016/S0191-8141(99)00061-9.

Hennings, P., 2009, AAPG-SPE-SEG Hedberg research conference on "The Geologic Occurrence and Hydraulic Significance of Fractures in Reservoirs." American Association of Petroleum Geologists Bulletin, v. 93, p. 1407–1412, doi:10.1306/intro931109.

Jolivet, L., Raimbourg, H., Avigad, D., and Leroy, Y., 2005, Softening triggered by eclogitization, the first step toward exhumation during continental subduction. Earth and Planetary Science Letters, v. 237, p. 532–547, doi:10.1016/j.epsl.2005.06.047.

Koban, C.G., and Schweigert, G., 1993, Microbial origin of travertine fabrics—Two examples from southern Germany (Pleistocene Stuttgart travertines and Miocene Riedöschingen travertine). Facies, v. 29, p. 251–263, doi:10.1007/BF02536931.

Koopman, A., 1983, Detachment tectonics in the central Apennines, Italy. Geologica Ultraiectina, v. 30, 155 p.

Larsen, B., and Gudmundsson, A., 2010, Linking of fractures in layered rocks: Implications for permeability. Tectonophysics, v. 492, p. 108–120, doi:10.1016/j.tecto.2010.05.022.

Larsen, B., Grunnaleite, I., and Gudmundsson, A., 2010, How fracture systems affect permeability development in shallow-water carbonate rocks: An example from the Gargano Peninsula, Italy. Journal of Structural Geology, v. 32, p. 1212–1230, doi:10.1016/j.jsg.2009.05.009.

Laubach, S.E., Olson, J.E., and Gross, M.R., 2009, Mechanical and fracture stratigraphy. American Association of Petroleum Geologists Bulletin, v. 93, p. 1413–1426, doi:10.1306/07270909094.

Madonna, R., Signanini, P., Crema, G., Di Sabatino, B., Rainone, M.L., and Di Nunzio, A., 2005, The geothermal area of Acquasanta Terme (central Italy): Main characteristics and an attempt of field evaluation, *in* Proceedings World Geothermal Congress 2005. Antalya, Turkey, International Geothermal Association, no. 2638, p. 8.

Maggi, M., Rossetti, F., Corfu, F., Theye, T., Andersen, T.B., and Faccenna, C., 2012, Clinopyroxene-rutile phyllonites from the East Tenda shear zone (Alpine Corsica, France): Pressure-temperature-time constraints to the Alpine reworking of Variscan Corsica. Journal of the Geological Society of London, v. 169, p. 723–732, doi:10.1144/jgs2011-120.

Maggi, M., Rossetti, F., Ranalli, G., and Theye, T., 2014, Feedback between fluid infiltration and rheology along a regional ductile-to-brittle shear zone: The East Tenda shear zone (Alpine Corsica). Tectonics, v. 33, p. 253–280, doi:10.1002/2013TC003370.

Mancini, E.A., Morgan, W.A., Harris, P.M., and Parcell, W.C., 2013, Introduction: AAPG Hedberg Research Conference on Microbial Carbonate Reservoir Characterization—Conference summary and selected papers. American Association of Petroleum Geologists Bulletin, v. 97, p. 1835–1847, doi:10.1306/intro070913.

Marsili, P., and Tozzi, M., 1995, Un livello di scollamento nella dorsale di Acquasanta (Ascoli Piceno). Bollettino della Società Geologica Italiana, v. 114, p. 177–194.

Martín-Chivelet, J., Palma, R.M., López-Gómez, J., and Kietzmann, D.A., 2011, Earthquake-induced soft-sediment deformation structures in Upper Jurassic open-marine microbialites (Neuquén Basin, Argentina). Sedimentary Geology, v. 235, p. 210–221, doi:10.1016/j.sedgeo.2010.09.017.

Mattei, M., Funiciello, R., and Kissel, C., 1995, Paleomagnetic and structural evidence for Neogene block rotations in the central Apennines, Italy. Journal of Geophysical Research, v. 100, p. 17,863–17,883, doi:10.1029/95JB00864.

Menichetti, M., 2008, Assetto strutturale del sistema geotermico di Acquasanta Terme (Ascoli Piceno). Rendiconti Online Società Geologica Italiana: Note Brevi, v. 1, p. 118–122.

Minissale, A., Kerrick, D.M., Magro, G., Murrell, M.T., Paladini, M., Rihs, S., Sturchio, N.C., Tassi, F., and Vaselli, O., 2002, Geochemistry of Quaternary travertines in the region north of Rome (Italy): Structural, hydrologic and paleoclimatic implications. Earth and Planetary Science Letters, v. 203, p. 709–728, doi:10.1016/S0012-821X(02)00875-0.

Mosegaard, K., and Tarantola, A., 2002, Probabilistic approach to inverse problems. International Geophysics, v. 81A, p. 237–265, doi:10.1016/S0074-6142(02)80219-4.

Nearing, M., Parker, S.C., Bradford, J.M., and Elliot, W.J., 1991, Tensile-strength of thirty-three saturated repacked soils. Soil Science Society of America Journal, v. 55, p. 1546–1551, doi:10.2136/sssaj1991.03615995005500060008x.

Ogniben, L., Parotto, M., and Praturlon, A., 1975, Structural Model of Italy. Maps and Explanatory Notes. Rome, Consiglio Nazionale delle Ricerche, scale 1:500,000, 502 p.

Olson, J.E., 2003, Sublinear scaling of fracture aperture versus length: An exception or the rule? Journal of Geophysical Research, v. 108, p. 2413, doi:10.1029/2001JB000419.

Ortega, O.J., Gale, J.F.W., and Marrett, R., 2010, Quantifying diagenetic and stratigraphic controls on fracture intensity in platform carbonates: An example from the Sierra Madre Oriental, northeast Mexico. Journal of Structural Geology, v. 32, p. 1943–1959, doi:10.1016/j.jsg.2010.07.004.

Pace, P., and Calamita, F., 2013, Push-up inversion structures v. fault-bend reactivation anticlines along oblique thrust ramps: Examples from the Apennines fold-and-thrust belt (Italy). Journal of the Geological Society of London, v. 171, p. 227–238, doi:10.1144/jgs2013-053.

Pentecost, A., 1995, The Quaternary travertine deposits of Europe and Asia Minor. Quaternary Science Reviews, v. 14, p. 1005–1028, doi:10.1016/0277-3791(95)00101-8.

Pentecost, A., 2005, Travertine. Berlin, Springer, 446 p.

Pentecost, A., and Viles, H., 1994, A review and reassessment of travertine classification. Géographie Physique et Quaternaire, v. 48, p. 305, doi:10.7202/033011ar.

Platt, N.H., and Wright, V.P., 1991, Lacustrine carbonates: Facies models, facies distributions and hydrocarbon aspects, *in* Anadn, P., Cabrera, L., and Kelts, K., eds., Lacustrine Facies Analysis. Oxford, UK, Blackwell Publishing Ltd., p. 57–74.

Pratt, B., 1998, Molar-tooth structure in Proterozoic carbonate rocks: Origin from synsedimentary earthquakes, and implications for the nature and evolution of basins and marine sediment. Geological Society of America Bulletin, v. 110, p. 1028–1045, doi:10.1130/0016-7606(1998)110<1028.

Principi, G., and Treves, B., 1984, Il sistema Corso-Appenninico come prisma d'accrezione. Riflessi sul problema generale del limite Alpi-Appennini. Memorie della Società Geologica Italiana, v. 28, p. 549–576.

Putnis, A., and Austrheim, H., 2010, Fluid-induced processes: Metasomatism and metamorphism. Geofluids, v. 10, p. 254–269, doi:10.1111/j.1468-8123.2010.00285.x.

Riding, R., 2011, Microbialites, stromatolites, and thrombolites, *in* Reitner, J., and Thiel, V., eds., Encyclopedia of Geobiology. Dordrecht, Netherlands, Springer, p. 635–654.

Royden, L., Patacca, E., and Scandone, P., 1987, Segmentation and configuration of subducted lithosphere in Italy: An important control on thrust-belt and foredeep-basin

evolution. Geology, v. 15, p. 714, doi:10.1130/0091-7613(1987)15<714:SACOSL>2.0.CO;2.

Salvini, F., 1993, Block tectonics in thin-skin style-deformed regions: Examples from structural data in central Apennines. Annali di Geofisica, v. 36, p. 97–109.

Salvini, F., and Vittori, E., 1982, Analisi strutturale della Linea Olevano-Antrodoco-Posta (Ancona-Anzio auct.): Metodologia di studio delle deformazioni fragili e presentazione del tratto meridionale. Memorie della Società Geologica Italiana, v. 24, p. 337–355.

Salvini, F., Billi, A., and Wise, D.U., 1999, Strike-slip fault-propagation cleavage in carbonate rocks: The Mattinata fault zone, Southern Apennines, Italy. Journal of Structural Geology, v. 21, p. 1731–1749, doi:10.1016/S0191-8141(99)00120-0.

Scisciani, V., and Calamita, F., 2009, Active intraplate deformation within Adria: Examples from the Adriatic region. Tectonophysics, v. 476, p. 57–72, doi:10.1016/j.tecto.2008.10.030.

Scisciani, V., Tavarnelli, E., and Calamita, F., 2002, The interaction of extensional and contractional deformations in the outer zones of the central Apennines, Italy. Journal of Structural Geology, v. 24, p. 1647–1658, doi:10.1016/S0191-8141(01)00164-X.

Storti, F., Salvini, F., and McClay, K., 1997, Fault-related folding in sandbox analogue models of thrust wedges. Journal of Structural Geology, v. 19, p. 583–602, doi:10.1016/S0191-8141(97)83029-5.

Tarantola, A., 2005, Inverse Problem Theory and Methods for Model Parameter Estimation. Philadelphia, Pennsylvania, Society for Industrial and Applied Mathematics, 352 p.

Tavani, S., Storti, F., Salvini, F., and Toscano, C., 2008, Stratigraphic versus structural control on the deformation pattern associated with the evolution of the Mt. Catria anticline, Italy. Journal of Structural Geology, v. 30, p. 664–681, doi:10.1016/j.jsg.2008.01.011.

Tenthorey, E., Cox, S.F., and Todd, H.F., 2003, Evolution of strength recovery and permeability during fluid–rock reaction in experimental fault zones. Earth and Planetary Science Letters, v. 206, p. 161–172, doi:10.1016/S0012-821X(02)01082-8.

Terra, G.J.S., and 18 others, 2009, Classificação de rochas carbonáticas aplicável às bacias sedimentares brasileiras. Boletim de Geociências da Petrobras, Rio de Janeiro, v. 18, p. 9–29.

Vignaga, E., Haynes, H., and Sloan, W.T., 2012, Quantifying the tensile strength of microbial mats grown over noncohesive sediments. Biotechnology and Bioengineering, v. 109, p. 1155–1164, doi:10.1002/bit.24401.

Witherspoon, P.A., Wang, J.S.Y., Iwai, K., and Gale, J.E., 1980, Validity of cubic law for fluid flow in a deformable rock fracture. Water Resources Research, v. 16, p. 1016–1024, doi:10.1029/WR016i006p01016.

Wright, V.P., 2012, Lacustrine carbonates in rift settings: The interaction of volcanic and microbial processes on carbonate deposition, *in* Garland, J., Neilson, J.E., Laubach, S.E., and Whidden, K.J., eds., Advances in Carbonate Exploration and Reservoir Analysis. Geological Society of London Special Publication 370, p. 39–47, doi:10.1144/SP370.2.

Xianghua, M., and Ming, G., 2002, The sedimentary features of Proterozoic microspar (molar-tooth) carbonates in China and their significance. Episodes, v. 25, p. 185–195.

Science Editor: Christian Koeberl
Associate Editor: Enrico Tavarnelli

Manuscript Received 16 July 2014
Revised Manuscript Received 17 October 2014
Manuscript Accepted 15 December 2014

Printed in the USA